Structural and Multidisciplinary Optimization (2021) 64:3653–3679
https://doi.org/10.1007/s00158-021-03046-3

RESEARCH PAPER

Reliability-based control co-design of horizontal axis wind turbines

Tonghui Cui[1] · **James T. Allison**[1] · **Pingfeng Wang**[1]

Received: 13 March 2021 / Revised: 3 August 2021 / Accepted: 5 August 2021 / Published online: 20 September 2021

Abstract
Wind energy is one of the fastest-growing energy sources due to its cleanness, sustainability, and cost-effectiveness. In the past, wind turbine design studies focused primarily on a sub-system or single-discipline design and analysis, including control, structural, aerodynamic, and electro-mechanical studies, for example. More recent studies formulated wind turbine design problems using multidisciplinary design optimization (MDO) strategies, with either static or dynamic system models, providing the potential for identifying system-level optimal designs. On the other hand, efforts have also been made to increase the reliability and robustness of wind turbines by accounting for various sources of uncertainty explicitly in the design process. In the presented study, the MDO formulation of wind turbine design problem has been extended to include both control system co-design and reliability considerations in an integrated manner. As a result, the optimal wind turbine design that has an optimal control solution and is robust to uncertainties can be obtained at an early design stage, which would benefit the controller design and maintenance design at latter phases. In this paper, the design of a horizontal axis wind turbine (HAWT) supported by a tubular tower is considered and formulated as a multi-objective control co-design problem with design parameter uncertainties and stochastic wind load. A physics-based multidisciplinary dynamic model of tubular-tower-supported pitch-controlled HAWT that captures the main design conflicts under extreme wind is provided and implemented, along with the necessary modifications to make nested control co-design comply with modern reliability-based design optimization structures, forming a new class of reliability-based co-design (RBCD) problems. In particular, we provide detailed discussions about RBCD problem formulations and implementation strategies, and with the HAWT design problem, we demonstrate the results and computational costs with integrated double-loop, single-loop, as well as decoupled methods.

Keywords Co-design · Reliability-based design optimization · Wind energy

1 Introduction

Ever since modern wind turbines were introduced in 1980s, we have seen continuous increases in tower heights and rotor sizes for capturing more wind energy at lower cost of energy. Although the growth in turbine sizes leads to increased energy capacity and reduced cost of energy, it also introduces growing costs on construction and maintenance. Such a trend is primarily driven by the facts that wind resource quality improves at higher altitudes and taller towers also allow larger size rotors to be used (Lantz et al. 2019). An intuitive design method to capture such a trend is upscaling, which increases the sizes of main turbine components following certain geometrical similarity rules (Sieros et al. 2012). However, the upscaling methods have difficulty to further reduce the cost of energy since they are based upon existing designs and their performances only, and therefore may experience limits in capturing the nonlinear multi-physics dynamics of the physically coupled components. Later studies seek improvements as they include dynamics of components and utilize Multi-disciplinary Design Optimization (MDO) techniques to resolve such a deficiency for either component-level design (Grujicic et al. 2010; Vasjaliya and Gangadharan 2013; Pavese et al. 2017) or system-level design (Maki et al. 2012; Deshmukh and Allison 2016; Ashuri et al. 2016; Forcier and Joncas 2012; McWilliam et al. 2018) while considering design uncertainties and system reliability (Li et al. 2017; Hu et al. 2013, 2016).

Responsible Editor: Jianbin Du

✉ Pingfeng Wang
pingfeng@illinois.edu

[1] University of Illinois at Urbana-Champaign, Urbana, IL 61801, USA

As an actuated dynamic system, the states of a wind turbine show dependency on both the plant and controller design. Traditionally, such a problem is solved sequentially, where the physical design is completed before the controller designs. This separation results in decoupled or weakly-coupled sub-problems and makes it challenging to discover the system-level optimal solution for the interconnected system. Meanwhile, the appearance of uncertainties in practical implementation adds extra difficulty by reducing the feasible control design space, where inactive constraints of the deterministic design may become active due to various sources of uncertainties. In such a scenario, the early-phase plant design may become more conservative than needed due to the lack of information about the actively controlled dynamics. Iterative methods are a potential alternative, but it is usually more costly in reality and it could fail to find the system-level optimum (Fathy et al. 2001; Allison and Nazari 2010). To meet the safety requirements of such engineering problems and balance the plant and control design efforts, system designers may formulate an optimization problem with probabilistic constraints, using reliability as the safety measurement with respect to an integrated physics and control design problem, or control co-design (CCD) problem. This type of problems consists of three tasks: plant design, controller design, and reliability assessment, which form a unique type of probability-constrained multidisciplinary design optimization problems. The plant design usually concerns decisions regarding the construction and sizing of a physical system; the controller design is related to sensing and regulating the dynamic behavior by feeding in proper control inputs, while the reliability assessment evaluates the likelihood of system failure considering various sources of uncertainty.

The above problem has been addressed partially by previous studies in two different areas, namely control co-design (CCD) and Reliability-based Design Optimization (RBDO). CCD is a special class of MDO problems where the coupled design disciplines include control system design and one or more plant (physical system) design disciplines (Allison and Herber 2014). Plant design involves determining the embodiment of the physical aspects of a system. Controller design relates to the sensing and regulating of dynamical system behavior by providing proper control inputs. Unlike conventional sequential design methods, where control design is performed after plant design is complete, co-design is an integrated approach that accounts fully for design coupling between plant and control design, producing a system-optimal result (Fathy et al. 2001). Numerous successful simulation-based implementations of co-design have been demonstrated. Fathy et al. showed successful implementation of nested co-design for a passive/active automotive suspension system (Fathy et al. 2003). Yan et al. demonstrated improved performance of a four-bar linkage powered by a variable-speed servo motor (Yan and Yan 2009). Allison et al. demonstrated application of both simultaneous and nested co-design for a robotic manipulator (Allison 2013), an active suspension (Allison et al. 2014), and horizontal axis wind turbines (Deshmukh and Allison 2016).

In recent years, co-design has been applied primarily in a deterministic manner, where open-loop control (OLC) is used as part of an integrated system design problem. Specifically, direct transcription (DT), a direct optimal control method that discretizes the infinite-dimensional optimal OLC problem to form a corresponding approximate nonlinear program (NLP), has been demonstrated to be an especially effective solution strategy (Herber and Allison 2019). Note that when OLC is adopted, the focus of CCD is to find a system-level optimal design in early design phase that would benefit planning and controller design at a later phase. In other words, the goal is to create a physical design that is capable of being controlled properly. While the OLC-based CCD methods provide quantitative system design insights, they do have limitations due to reliance on OLC, such as practical implementation for later design phases. Efforts have also been made to address the practical limitations, including the development of system-optimal closed-loop control (CLC) designs based on OLC-based CCD results (Deshmukh et al. 2015) and CCD for stochastic dynamic systems utilizing the stochastic Hamilton–Jacobi–Bellman (sHJB) equation (Cui et al. 2020b).

Another challenge in practical implementation is uncertainty, which appears in modeling, measurements, and environments. While considering uncertainties in system design optimization, probabilistic design formulations can generally be applied, such as the RBDO, Possibility-based Design Optimization (PBDO), or Robust Design Optimization (RDO) (Fan et al. 2019; Jiang et al. 2021; Zhang et al. 2020; Lee et al. 2019, 2020; Hu and Du 2015; Du et al. 2008; Park et al. 2015). In standard RBDO formulations, uncertainty-induced failures can be quantified as probability of failure. Various strategies have been presented in the literature to evaluate the probability of failure efficiently. For example, Tu et al. presented a general probabilistic constraint evaluation for RBDO and compared the performance of the Reliability Index Approach (RIA) and Performance Measurement Approach (PMA) (Tu et al. 1999). A Hybrid Mean Value method was introduced to handle concave problems for the slow convergence of the Conjugate Mean Value method, and a modified version was proposed to handle nonlinearities in Youn et al. (2003) and Youn et al. (2005). To compare several first-order approximate methods, Chiralaksanakul and Mahadevan compared their efficiency, accuracy, and convergence through numerical examples (Chiralaksanakul and Mahadevan 2005). In the case of correlated inputs, Noh provided a method that converts dependent input variables to independent standard normal variables using the Gaussian

copula (Noh et al. 2009). The studies described above all use double-loop formulations, where design optimization (DO) and reliability analysis(RA) are nested. Likewise, single-loop methods (Liang et al. 2007; Nguyen et al. 2010) and decoupled methods, such as Sequential Optimization and Reliability Assessment (SORA) (Du and Chen 2004) have also been proposed to reduce the computational burden.

While significant advancements have been made recently in co-design and RBDO separately, limited work has been done to integrate reliability-based design optimization for control co-design of dynamic systems. Cui et al. proposed a Reliability-based Co-design (RBCD) framework for Linear Quadratic (LQ) problems with double-loop methods for Reliability Assessment (RA) (Cui et al. 2020a). Azad and Alexander-Ramos presented reliability-based co-design for nonlinear problems using SORA (Azad and Alexander-Ramos 2020). The earlier works attempted to use different reliability assessment strategies to show efficacy of RBCD and reduce its computational cost, it is yet to see a real-world application to provide evidence for its value and reveal more practical challenges. Also, a real-world application can serve as a test bed for developing innovative algorithms for RBCD. In this paper, we focus on the RBDO implementation for horizontal axis wind turbine (HAWT) co-design, in the presence of aleatory design uncertainties and stochastic wind load. The rest of this paper is organized as follows: Section 2 covers details regarding dynamics of the HAWT subsystems. The proposed method for reliability-based co-design of HAWT in the presence of parametric and dynamic uncertainties is presented in Sect. 3. Section 4 discusses the results of the probability-constrained problem and compares them with the deterministic results. Finally, Sect. 5 concludes the paper and describes future opportunities for related studies.

2 HAWT dynamic model

Control co-design brings design optimization of the physical system and the control decisions together. To achieve that, it requires the model to (1) capture the controlled dynamics and the coupling among different disciplines; (2) reflect the change in physically meaningful design variables; and (3) be as simple as possible such that optimal control and design optimization problems can be solved efficiently. Both optimal control and design optimization problems become challenging for high-dimensional systems, the accumulated computational cost could be prohibitively high. To meet the three requirements, we may use first principle models or hybrid physics-surrogate models. A first principle model is based on established physical laws and assumes no fitting parameters. This brings an obvious benefit that the dynamics can be updated directly when the physical design changes. However, it is essential to select the models wisely for a multidisciplinary problem since some first principle models themselves are difficult to evaluate. There are also simplified physics-based models that capture the dynamics and are easy to evaluate. However, they may be not coupled with physically meaningful design variables. In that case, it is possible to establish the coupling effect by adopting surrogate models. The downside of hybrid physics-surrogate modeling is the introduction of the sample-based modeling sub-problem (Cui et al. 2020c). We choose the first strategy for this study and balance its computational cost through model management.

In this study, we optimize an upwind, 3-bladed, tubular tower supported, 5 MW horizontal axis wind turbine, which is composed of the rotor (blades and the hub) with pitch control, the low-speed shaft on the rotor side, the gearbox, the high-speed shaft on the generator side, the generator, and the tubular tower, shown in Fig. 1. The task is making design and control decisions concurrently for a system-level optimal solution. Specifically, we study the trade-off between more abundant wind energy at increased height above ground and the increased cost of the wind turbine tower. Tower design optimization and pitch angle optimal control are solved in a co-design framework, with considerations of the multidisciplinary dynamics of all the components mentioned above and the reliability issue elevated by the increased wind load. Several simplifications are made to reduce the model complexity while seizing the coupling effect associated with the design conflict between the cost and energy production. We suppress the yaw motion of the nacelle by assuming a constant wind direction that flowing toward the rotor, as well as the structural strength of the blades since we are interested in the tower geometries only. Besides, wind turbines are usually operated differently as the wind velocity changes. In the low-speed region, the wind load, thrust force in particular, is not large enough to activate structural constraints of

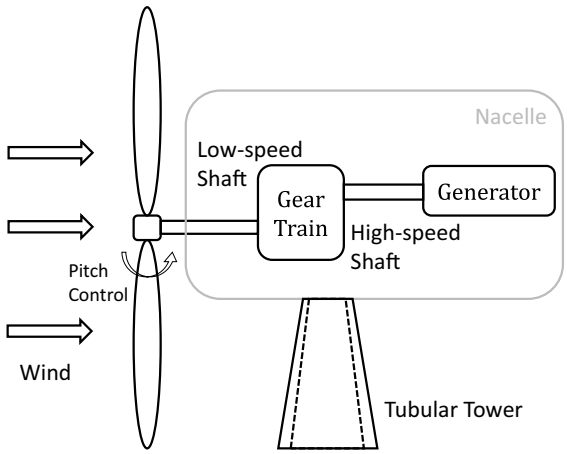

Fig. 1 Simplified wind turbine diagram

the tower dynamics. As a result, the design coupling effect between the tower design and the pitch control will become minimum due to the loss of activeness in the important constraints. Hence, we assume the wind turbine operates in its pitch-controlled region, where the wind velocity is high (greater than 12 m/s, for example). Also, instead of using the commonly adopted control strategy at high wind speed where generator RPM is kept constant through pitch control, we formulate a constrained optimal control problem for all the coupled dynamics. This allows us to gain more insights into the design coupling effect between the tower design and the pitch control.

Regarding the model selection, the multidisciplinary design problem concerns aerodynamics of the rotor, transmission from the rotor (low-speed end) to the generator (high-speed end), electro-mechanical dynamics of the generator, and structural dynamics of the tower. Since the plant design variables are related to the tower geometries and the pitch control is related to the rotor aerodynamics. We adopt physics-based models that can be updated and evaluated as the design and control variables change. Since the wind speed is a height-dependent, time-varying, stochastic input to the aerodynamics, a spatial-temporal model is created that can generate time series of wind speed that follows the stochastic distribution of the local wind. We choose simple physics-based models for the transmission and generator dynamics since their models are not directly coupled with the physically meaning design and control variables. Following these guidelines, we generate dynamic models for each of the subsystems, and the model parameters are either fixed or can be derived analytically and based on physical design variables.

2.1 Wind speed model

Both energy production and load on the structure are dependent upon the wind speed. The wind speed is coupled with the height above ground and follows a site-specific Weibull distribution. As the height above ground increases, the pressure gradient increases, while the friction due to ground surface and the air density decreases, which contribute to an increased wind velocity. Along with the aerodynamics of the rotor, the wind speed model creates a major design conflict that the rotor harvests more energy at higher altitude, but it also adds more load to the structure, which boosts structure cost. The current control co-design framework solves an OLC problem in the time domain, which takes wind speed input as a time series. Earlier wind turbine control co-design work (Deshmukh and Allison 2016) evaluates power production as an integral between cut-in and cut-off wind speed over a distribution, which does not provides insights about load and energy production in the time domain. In this work, a sample wind speed can be generated as an altitude-dependent time series that follows a Weibull distribution. In particular, the wind speed model (1) follows a site-specific Weibull distribution that is parameterized based on actual wind measurements; (2) shows spatial dependency on the hub height above ground; (3) can be used to generates wind profiles repeatedly to account for its randomness.

One method to generate a time series model based on its past values is Auto Regressive Integrated Moving Average (ARIMA) (Box and Jenkins 1970). It models the differences as a linear combination of its lagged values as well as lagged forecast errors. The original model assumes a Gaussian error term, which differs from the generally accepted Weibull distribution of wind speeds (He et al. 2010). This drawback can be overcome by applying a power transformation that truncates the wind distribution to Gaussian (Sim et al. 2019). The optimal power coefficient can be solved numerically based on the wind data. The original work was based on offshore wind speed measurement. To adapt it for land-based wind turbines, we may use the wind data provided by the National Wind Technology Center (NWTC), measured at their 135 m M5 tower. Wind speed measurements are provided at several different heights (NWTC 2020). Specifically, we used the wind speed data between January 1st to January 31st in 2019, measured at 30 m, 55 m, 80 m, 105 m, and 130 m by cup-type anemometers to build the height-dependent ARIMA model. NWTC also provides more accurate wind data measured by sonic anemometers, but additional work is needed to compensate for their higher rates of fault and missing data. The exemplary wind data measured at 30 m, 80 m, and 130 m are shown in Fig. 2.

The optimal power coefficient can be obtained by following the method proposed in Sim et al. (2019). As suggested, a power transformation can be taken for the wind speed.

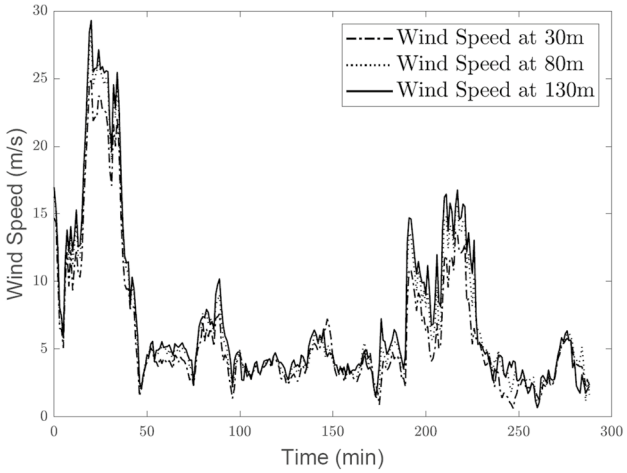

Fig. 2 Sample wind data at M5 provided by NWTC

Such an operation results in a Gaussian-like distribution and therefore makes it suitable for an ARIMA model. The type of ARIMA model adopted is (0, 1, 2), or a damped Holt's model. The corresponding model coefficients and Weibull coefficients are summarized in Table 1.

Here α_* is the optimal power transform coefficient, β and λ are Weibull distribution parameters, and θ and ν are ARIMA coefficients. The coefficients at different heights are interpolated by second-order polynomials. After that, the wind profile at an arbitrary height can be generated as a function of height, time, and initial speed at the reference height, after taking the inverse power transform to recover the wind speed, U_{inf}. We may summarize the model as:

$$U_{\text{inf}} = f_{\text{wind}}\{t, L, v_{\text{w0}}\}, \tag{1}$$

where t is the time, L is the hub height above ground, v_{w0} is the initial wind speed at the reference height.

2.2 Rotor aerodynamics

When only power output and wind thrust of an ideal turbine rotor are considered, the rotor can be modeled using the well-established actuator disk model, which suppresses all geometric design elements except the swept area. The actuator disk model is simple to implement but not necessarily ideal for control co-design due to an internal conflict between its suppressed design parameters and its dependency on its performance curves. The performance curves are used to map the wind speed, pitch angle, and rotor velocity to its power coefficient, which is fixed to specific geometric rotor designs. Since the design parameters (except the swept area) are not shown in the model, the performance curves cannot be easily updated within the CCD framework. To resolve this issue, a model based on Blade Element Momentum (BEM) theory can be used to predict rotor performances with specific geometric design parameters for ideal, steady operating conditions. BEM divides a blade of radius R into several sections, each section is referred as a blade element, as shown in Fig. 3. It assumes no aerodynamic interaction among different sections, and therefore the aerodynamics are solely determined by the section geometries, lift coefficients, and drag coefficients. A database for the lift and drag coefficients for candidate airfoils should be available to apply the BEM method. Note that a model based on BEM can be updated with different designs of turbine blades, with respect to parameters such as blade element radial distance, r, element length, dr, chord length, c, prebent angle, and the chosen airfoil, which allows design optimization for blade design. For this study, we assume a fixed design of rotor blades; as a result, the corresponding thrust and torque applied by the wind can be expressed as functions of wind speed, rotor speed, and pitch angles.

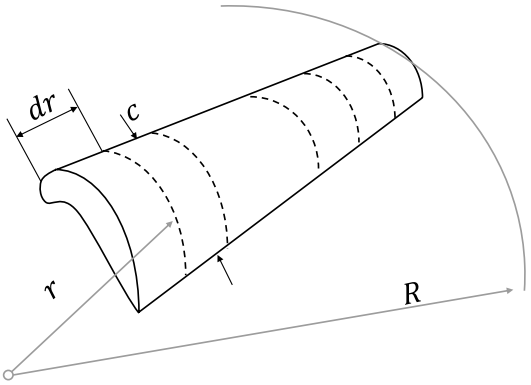

Fig. 3 Blade element model used in blade element momentum theory

The adopted rotor design follows the conceptual design of the 5 MW wind turbine developed by NREL (Jonkman 2009). The tech report provides design parameters, such as chord length and airfoil of the rotor blade sections. In addition, the variation of lift and drag coefficients for each airfoil is provided as a look-up table. Therefore, the functional dependence of steady-state rotor thrust and torque on wind speed, rotor speed, and pitch angles can be defined using look-up tables can be defined using look-up tables. Details of the parameters can be found in "Appendix 1". Note that the look-up tables correspond to steady-state response only. The transient responses are not provided and may be obtained using Computational Fluid Dynamics (CFD).

The sectional thrust, dT, and the sectional torque, dQ, applied to blade sections are estimated based on Kulunk (2011):

$$\mathrm{d}T = 4\pi\rho\Omega^2 a'(1+a')r^3\mathrm{d}r, \tag{2}$$

$$\mathrm{d}Q = 4\pi\rho U_{\text{inf}}\Omega a'(1-a)r^3\mathrm{d}r, \tag{3}$$

Table 1 Weibull parameters and ARIMA coefficients

Height (m)	α_*	β	λ	$\theta(1)$	$\theta(2)$	ν
30	0.48	1.41	5.35	5.49e−2	− 5.76e−2	5.43e−2
55	0.46	1.36	5.67	7.48e−2	− 5.15e−2	4.91e−2
80	0.44	1.33	5.88	8.74e−2	− 5.14e−2	4.48e−2
105	0.43	1.31	6.04	9.27e−2	− 5.73e−2	4.14e−2
130	0.43	1.30	6.16	9.06e−2	− 6.91e−2	3.90e−2

ρ, the air density, is assumed to be a constant 1.225 kg/m^3. Ω is the rotor angular velocity. U_{inf} is the wind speed provided by the wind model. r and dr denote the radial distance from the center of hub and the section length, and a and a' are the axial induction factor and angular induction factor, which can be calculated as:

$$a = \frac{1}{1 + 4\sin^2\phi/(\sigma C_{\text{L}})\cos\phi}, \tag{4}$$

$$a' = \frac{1}{4\cos\phi/(\sigma C_{\text{L}}) - 1}, \tag{5}$$

where ϕ is the angle of relative wind.The solidity ratio, σ, is defined as:

$$\sigma = \frac{Bc}{2\pi r} \tag{6}$$

where B is the number of blades and c is the chord length. The induction factors are correlated by

$$\frac{a(1-a)}{a'(1+a')} = \frac{\Omega^2 r^2}{U_{\text{inf}}^2} \tag{7}$$

The lift coefficient, C_{L}, is a function of angle of attack. This function depends on the specific airfoil used as detailed in "Appendix 1". The summation of angle of attack, pre-bent angle of each section, and pitch angle gives the angle of relative wind. The above equations can be solved for sectional thrust and torque, and the total thrust and torque on the rotor is the integration of sectional load over the entire blade length. Note that the pre-bent angles, cord length, section length and radius, air foils and the corresponding lift and drag coefficients are obtained from Jonkman 2009. According to the reference, the innermost nodes, 1–3, are cylinders with zero lift coefficient. This causes division by zero in Eqs. 4 and 5, and therefore should be calculated separately by decomposition of the drag force. We may summarize the model as:

$$[Q, T] = f_{\text{aero}}\{t, U_{\text{inf}}, x_{\text{c}}, \Omega\}, \tag{8}$$

where x_{c} represents the pitch angle control input. To further reduce the computational cost of solving the systems of equation in co-design and reliability assessment, the corresponding thrust force, T, and rotor torque, Q, can be solved off-line as functions of wind velocity, rotor angular velocity, and pitch angle. The results can be captured as response surfaces so that they can be referred efficiently during the optimization process. We show a sample result of the thrust and torque load at $U_{\text{inf}} = 20$ m/s, $x_{\text{c}} = 10°$, and $\Omega = 13$ rpm (Fig. 4).

2.3 Tower design and structural dynamics

The turbine tower is designed as a tubular tower shown below in Fig. 5, and characterized by its height, L, the height of the cone after extending the sides until they meet, L_1, the inner diameter of the tower base, $d_{1\text{i}}$, and the outer diameter of the tower base, d_1, assuming that the cones shaped by extensions of the inner and outer sides meet at the same point.

The structural dynamics of the tower can be obtained through Finite Element Analysis (FEA) methods. This usually leads to high dimensional dynamics and potential difficulty in solving the optimal control problem. In addition, FEA mesh may need updating with each new tower design, which introduces non-smoothness and difficulty in using gradient-based optimization methods. The tower can be simplified as a tapered hollow wedge beam with circular cross-sections and a point load at the tip. As suggested in

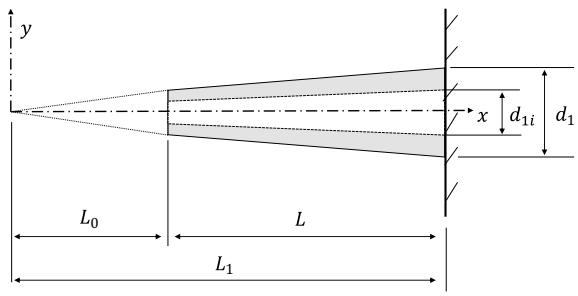

Fig. 5 Tubular tower design

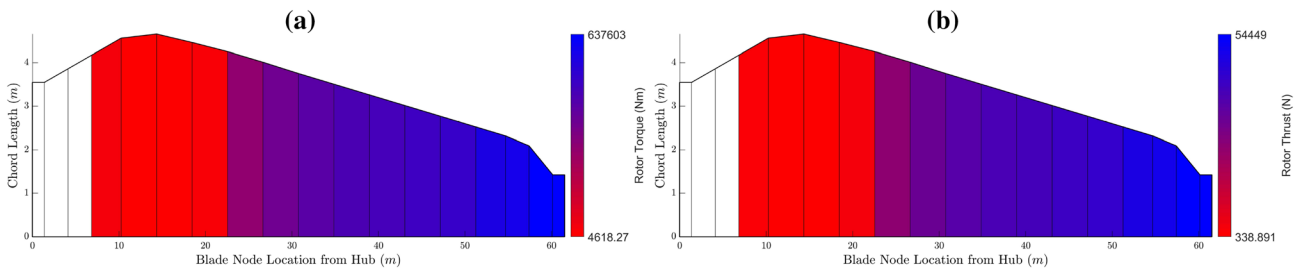

Fig. 4 Torque (**a**) and thrust (**b**) load of the rotor at $U_{\text{inf}} = 20$ m/s, $x_{\text{c}} = 10°$, and $\Omega = 13$ rpm

Wu and Chiang (2004), we may consider the tubular tower as an Euler–Bernoulli beam characterized by the following equation of motion:

$$\frac{\partial^2}{\partial x^2}\left(EI(x)\frac{\partial^2 y(x,t)}{\partial x^2}\right)+\rho A(x)\frac{\partial^2 y(x,t)}{\partial t^2}=0, \tag{9}$$

where x is the axial coordinate, y is the transverse deflection, E is the Young's modulus, ρ is the density of the tower material, $A(x)$ is the cross-section area, $I(x)$ is the moment of inertial at x, and t is time. For free vibration, the transverse deflection can be written in the form:

$$y(x,t)=W(x)e^{i\omega t}, \tag{10}$$

where W is the deflection amplitude and ω is the natural frequency. The cross-section area and the corresponding moment of inertial can be rewritten in the forms:

$$A(\epsilon)=A_1\epsilon^n \tag{11}$$

and

$$I(\epsilon)=I_1\epsilon^{n+2} \tag{12}$$

where:

$$A_1=\pi(d_1^2-d_{i1}^2)/4, \tag{13}$$

$$I_1=\pi(d_1^4-d_{i1}^4)/64, \tag{14}$$

$$\epsilon=\frac{x}{L_1}, \tag{15}$$

Then the following amplitude function can be used with Eq. 9:

$$W(\epsilon)=L_1^{-n/2}\epsilon^{-n/2}[c_1J_n(z)+c_2Y_n(z)+c_3I_n(z)+c_4K_n(z)], \tag{16}$$

where J_n and Y_n are the nth order Bessel functions of the first and second kind, I_n and K_n are the nth order modified Bessel functions of the first and second kind and z is a parameterization of the natural frequency, ω, which is defined as:

$$z=2\beta\epsilon^{\frac{1}{2}}, \tag{17}$$

$$\beta^4=\omega^2L_1^4\left(\frac{\rho A_1}{EI_1}\right). \tag{18}$$

For a free-clamped tapered beam, the boundary conditions are:

$$\frac{\partial^2 W}{\partial\epsilon^2}=\frac{\partial}{\partial\epsilon}\left(EI(\epsilon)\frac{\partial^2 W}{\partial\epsilon^2}\right)=0 \text{ at } \epsilon=\frac{L_0}{L_1} \tag{19}$$

$$W=\frac{\partial W}{\partial\epsilon}=0 \text{ at } \epsilon=1 \tag{20}$$

Substituting Eq. 16 into the boundary conditions yield a system of linear equations, Eqs. 21–24.

$$c_1J_3(z_0)+c_2Y_3(z_0)+c_3I_3(z_0)-c_4K_3(z_0)=0, \tag{21}$$

$$c_1J_4(z_0)+c_2Y_4(z_0)+c_3I_4(z_0)+c_4K_4(z_0)=0, \tag{22}$$

$$c_1J_2(z_1)+c_2Y_2(z_1)+c_3I_2(z_1)+c_4K_2(z_1)=0, \tag{23}$$

$$c_1J_3(z_1)+c_2Y_3(z_1)-c_3I_3(z_1)+c_4K_3(z_1)=0, \tag{24}$$

Setting the determinant of this linear system matrix to zero and identifying non-trivial solutions result in identification of natural frequencies, ω_r, and their corresponding mode shapes, W_r:

$$\omega_r=\left(\frac{\beta_r}{L_1}\right)\sqrt{\frac{EI_1}{\rho A_1}}, \tag{25}$$

$$W_r(\epsilon)=L_1^{-1}\epsilon^{-1}\left[c_1J_2(z_r)+c_2Y_2(z_r)\quad+c_3I_2(z_r)+c_4K_2(z_r)\right], \tag{26}$$

The analytical solutions are compared with modal frequency analysis generated using Finite Element Analysis (FEA) for sample tower designs (Fig. 6. The corresponding results are summerized in Table 2.

Clearly, discrepancies exist between the analytical solutions and the FEA solutions. However, the analytical results can correctly capture the trend of variation and can be efficiently updated, which makes them ideal for co-design and RBCD in early design phases. The analytical natural frequencies and mode shapes can be used to reconstruct the structural dynamics of the tapered tubular tower as described by Eqs. 9 and 10. We can superpose the rotor and nacelle mass and the thrust load for the externally loaded case with a centered mass on the tip of the tower. We may summarize the model as:

$$[x,\dot{x}]=f_{\text{tower}}\{t,T,\boldsymbol{x}_{\mathbf{p}}\}, \tag{27}$$

where x and $\dot{x}$ are the motion and its derivative of associated nodes.

2.4 Drive-train and generator dynamics

The drive-train can be modeled as a simple rotary shaft with equivalent stiffness, damping, and inertia calues, which are all available in Jonkman (2009). The 5 MW Doubly Fed Induction Generator (DFIG) is not detailed in the NREL tech report, but a dynamic model can be inferred for the pitch-controlled mode. The generator is operated at the nominal power rate when the wind turbine in Region 3, that is, when

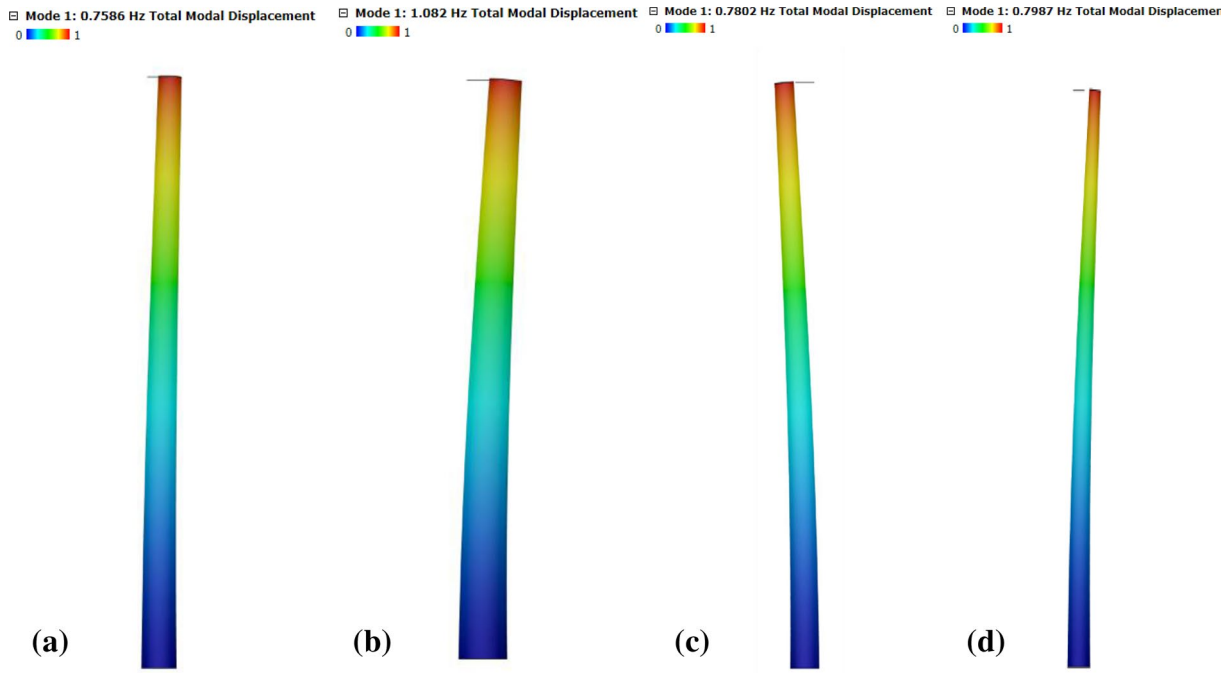

Fig. 6 FEA results for sample tower designs: **a** $\boldsymbol{x}_{\mathbf{p}} = [100, 300, 7, 6.8]$, **b** $\boldsymbol{x}_{\mathbf{p}} = [100, 300, 10, 9.8]$, **c** $\boldsymbol{x}_{\mathbf{p}} = [100, 300, 7, 6.9]$, **d** $\boldsymbol{x}_{\mathbf{p}} = [100, 200, 7, 6.8]$

Table 2 FEA and analytical modal analysis results

Sample	L (m)	L_1 (m)	d_1 (m)	d_{1i} (m)	FEA result (Hz)	Analytical result (Hz)
a	100	300	7	6.8	0.7586	0.8006
b	100	300	10	9.8	1.082	1.1468
c	100	300	7	6.9	0.7802	0.8063
d	100	200	7	6.8	0.7987	0.8931

the mean wind velocity is above $12m/s$. In this region, the generator torque can be modeled as inversely related to its angular velocity. A time constant can be added to turn the steady-state response into a first-order dynamic model based on available generator parameters:

$$\dot{\Omega} = \frac{1}{I_{\text{rot}}}\left(Q - \phi K_{\text{shaft}} - \dot{\phi} B_{\text{shaft}}\right), \tag{28}$$

$$\dot{\omega} = \frac{1}{I_{\text{gen}}}\left(-M_{\text{gen}} + \frac{1}{N}(\phi K_{\text{shaft}} + \dot{\phi} B_{\text{shaft}})\right), \tag{29}$$

$$\dot{\phi} = \Omega - \frac{1}{N}\omega, \tag{30}$$

where ω is the generator angular velocity. M_{gen} represents the generator torque. K_{shaft} and B_{shaft} are the shaft stiffness and damping constants. N is the gear ratio.

The generator is modeled as:

$$\dot{M}_{\text{gen}} = \frac{1}{\tau_{\text{gen}}}\left(\frac{P_{\text{ref}}}{\omega} - M_{\text{gen}}\right), \tag{31}$$

where τ_{gen} and P_{ref} are the time constant and the rated power of the generator. Following the reference control strategy, we assume pitch control is only activated in the high wind speed region, whereas it remains zero in the low-speed region.

3 Reliability-based control co-design of HAWT

The HAWT is a multidisciplinary system, concerning aerodynamic design regarding the rotor blades, structural design of the tower, blade, and drive-train, electro-mechanic design of the generator. In this work, the tower geometry and blade pitch control are optimized. Although the drive-train and the generator are not design subjects, they are essential components that place dynamic constraints on the system

optimization. In this section, we provide a general reliability-based co-design formulation first. Then we present the HAWT RBCD formulation in the presence of parametric uncertainty and loading uncertainty. In particular, we adopt the nested co-design formulation for the convenience of model updates, in which the reliability assessment is implemented in the outer loop. A double-loop (DLP) method using the Performance Measurement Approach (PMA), a single-loop (SLP) method , and a decoupled method using SORA are implemented for comparison of different RBCD performances.

3.1 General nested formulation of reliability-based control co-design

Let $\mathbf{x}_\mathrm{p}$, $\boldsymbol{\xi}$, and $\mathbf{x}_\mathrm{c}$ denote the set of physical system design variables, state trajectories, and the control inputs, respectively. Both control and state are functions of time, t. The dynamic model is defined as follows:

$$\dot{\boldsymbol{\xi}} - \mathbf{f}\left(t, \boldsymbol{\xi}(t), \mathbf{x}_\mathrm{c}(t), \mathbf{x}_\mathrm{p}\right) = \mathbf{0}, \tag{32}$$

In a direct optimal control problem, we seek to minimize a cost function that depends on dynamic system behavior, with respect to the infinite-dimensional control input trajectories, $\mathbf{x}_\mathrm{c}(t)$. An example of a cost function over a finite time horizon is:

$$J\left(\mathbf{x}_\mathrm{c}(t)\right) = \int_{t_0}^{t_f} O\left(t, \boldsymbol{\xi}(t), \mathbf{x}_\mathrm{c}(t)\right) dt + R\left(t_f, \boldsymbol{\xi}_f\right), \tag{33}$$

where $O(\cdot)$ defines the running cost, and $R(\cdot)$ is the terminal cost, i.e., the cost of reaching a specific final state $\boldsymbol{\xi}_f$ at the final time t_f (Liberzon 2011).

Optimal control problems may include several types of constraints, including time-independent constraints, state and path constraints that limit the state and control trajectories, and boundary conditions that define the initial and final states (e.g., for periodic optimal control). In co-design, system performance is optimized not only with respect to control input design, but also with respect to physical system design.

We may consider a nested formulation, where the RBCD problem can be formulated as a deterministic plant design problem in the outer loop, and reliability-based optimal control design in the inner loop. For normally-distributed random design variables $(\mu_{x_\mathrm{p}}, \sigma_{x_\mathrm{p}})$, the problem can be formulated as follows:

$$\begin{aligned} \min_{\boldsymbol{\mu}_{x_\mathrm{p}}} \quad & \theta\left(t, \boldsymbol{\xi}_*(t, \boldsymbol{\mu}_{x_\mathrm{p}}), \mathbf{x}_{\mathrm{c}*}(t, \boldsymbol{\mu}_{x_\mathrm{p}}), \boldsymbol{\mu}_{x_\mathrm{p}}\right) \\ \text{subject to} \quad & \mathbf{G}_\mathrm{F}\left(\boldsymbol{\mu}_{x_\mathrm{p}}\right) \le \mathbf{0} \\ & \boldsymbol{\mu}_{x_\mathrm{p}}^{\mathrm{Lo}} \le \boldsymbol{\mu}_{x_\mathrm{p}} \le \boldsymbol{\mu}_{x_\mathrm{p}}^{\mathrm{Up}}, \end{aligned} \tag{34}$$

where $\mathbf{x}_{\mathrm{c}*}(t, \boldsymbol{\mu}_{x_\mathrm{p}})$ and $\boldsymbol{\xi}_*(t, \boldsymbol{\mu}_{x_\mathrm{p}})$ refer to the optimal control and the corresponding state trajectories determined by the inner loop, which is defined in Eq. (35):

$$\begin{aligned} \min_{\mathbf{x}_\mathrm{c}(t), \boldsymbol{\xi}(t)} \quad & \theta\left(t, \boldsymbol{\xi}(t, \boldsymbol{\mu}_{x_\mathrm{p}}), \mathbf{x}_\mathrm{c}(t, \boldsymbol{\mu}_{x_\mathrm{p}}), \boldsymbol{\mu}_{x_\mathrm{p}}\right) \\ \text{subject to} \quad & \dot{\boldsymbol{\xi}} - \mathbf{f}\left(t, \boldsymbol{\xi}(t), \mathbf{x}_\mathrm{c}(t), \boldsymbol{\mu}_{x_\mathrm{p}}\right) = \mathbf{0} \\ & Pr\left(\mathbf{G}\left(t, \boldsymbol{\xi}(t), \mathbf{x}_\mathrm{c}(t), \boldsymbol{\mu}_{x_\mathrm{p}}\right) \le \mathbf{0}\right) \ge \Phi(\beta^t), \end{aligned} \tag{35}$$

where θ represents the general cost function, Φ is the cumulative distribution due to the standard normal distribution, and β^t is the target reliability level. Here, the feasibility constraint $\mathbf{G}_\mathrm{F}(\cdot)$ must enforce non-emptiness of inner loop reliable optimal control solutions. The inner loop is an optimal control problem with probability constraints, which suffers from the computational cost induced by reliability assessment and optimal control. Earlier work (Cui et al. 2020a) shows that the computational burden can be alleviated by choosing an intuitive yet trivial feasibility constraint, $\mathbf{G}_\mathrm{F}(\cdot)$, as the probability constraint, $Pr\left(\mathbf{G}\left(t, \boldsymbol{\xi}_*(t), \mathbf{x}_{\mathrm{c}*}(t), \boldsymbol{\mu}_{x_\mathrm{p}}\right) \le \mathbf{0}\right)$. Having the reliability constraint in the outer loop, we may relax the inner loop reliability constraint by using a deterministic constraint evaluated at the mean value of design, $\mathbf{G}\left(t, \boldsymbol{\xi}(t), \mathbf{x}_\mathrm{c}(t), \boldsymbol{\mu}_{x_\mathrm{p}}\right)$. We further define F_G as the CDF of $G(\cdot)$, such that:

$$F_\mathrm{G} = Pr\left(\mathbf{G}\left(t, \boldsymbol{\xi}_*(t), \mathbf{x}_{\mathrm{c}*}(t), \boldsymbol{\mu}_{x_\mathrm{p}}\right) \le \mathbf{0}\right) \tag{36}$$

Note that $G(\cdot)$ is time-dependent and requires simulations of the dynamics for evaluation. The limit state function of a time-dependent problem can be considered as a limit state function at each time step. Therefore, they are only activated at the time steps where constraints are not satisfied. we choose the infinity norm of the constraint violation as the G value. When the simulation results of the trajectories show no violation of the constraints, the G value is zero. When the simulation results show violation of any constraints (not necessarily for one constraint), the maximum absolute value between the state/path and their constraints is taken as G. The reliability constraint evaluated using PMA can be formulated as follows:

$$G^\mathrm{p} = F_\mathrm{G}^{-1}\left(\Phi(\beta^t)\right) \le 0 \tag{37}$$

Here, F_G^{-1} represents the inverse transformation. To solve for G^p, the first-order estimate is obtained by solving the following optimization problem in the U-space:

$$\begin{aligned} \min_{\mathbf{U}} \quad & G(\mathbf{U}) \\ \text{subject to} \quad & ||\mathbf{U}|| = \beta^t \end{aligned} \tag{38}$$

where the constraint in the above problem defines the target reliability surface. The MPP, $\mathbf{u}^*$, is the point on the target reliability surface that maximizes the constraint function in the U-space, $g(\cdot)$, where $G(\mathbf{u}) \equiv G\left(\boldsymbol{x}_{\mathbf{p}}(\mathbf{u})\right)$.

3.2 Double-loop RBCD formulation of HAWT

Wind turbine design problems are typically formulated as bi-objective: maximizing energy production and minimizing construction cost. Since we are only considering turbine operation under the pitch-controlled high-speed region, the generator is assumed to operate under a constant magnetic field (fixed field excitation current). The optimization variables include the pitch angle trajectory x_{c}, tower geometry parameters $x_{\mathrm{p}} = \left[L, L_1, d_1, d_{1i}\right]^T$, and state variables $\xi(t) = \left[y_{\mathrm{L}}(t), \dot{y}_{\mathrm{L}}(t), \Omega(t), \omega(t), \phi(t), M_{\mathrm{gen}}(t), \beta(t), \dot{beta}(t)\right]^T$. The tower geometry parameters are assumed to follow normal distributions. Their normalized values have a standard deviation of 0.1. The exact numbers can be modified based on manufacturing statistics. Constraints include dynamics as introduced in Sect. 2, state constraints, path constraints, and plant constraints. State constraints refer to the bounds of the state and control trajectories, while path constraints are functions of states. For this work, we consider the tip deflection as the only active path constraint for simplicity purpose, and all the states are bounded based on values presented in the turbine reference. We adopt the weighted sum of the two objectives as the objective:

$$\theta_{\mathrm{HAWT}}\left(t, \boldsymbol{\xi}(t, \boldsymbol{\mu}_{\boldsymbol{x}_{\mathbf{p}}}), \mathbf{x}_{\mathrm{c}}(t, \boldsymbol{\mu}_{\boldsymbol{x}_{\mathbf{p}}}), \boldsymbol{\mu}_{\boldsymbol{x}_{\mathbf{p}}}\right) = w_1 \int_{t_0}^{t_{\mathrm{f}}} M_{\mathrm{gen}} \omega \mathrm{d}t + w_2 V_{\mathrm{tower}}, \tag{39}$$

where V_{tower} is the volume of the tapered tubular tower and w_1 and w_2 are objective function weights. The inner loop optimal control problem is formulated as:

$$\begin{aligned} \min_{\mathbf{x}_{\mathrm{c}}(t), \boldsymbol{\xi}(t)} \quad & \theta_{\mathrm{HAWT}}\left(t, \boldsymbol{\xi}(t, \boldsymbol{\mu}_{\boldsymbol{x}_{\mathbf{p}}}), \mathbf{x}_{\mathrm{c}}(t, \boldsymbol{\mu}_{\boldsymbol{x}_{\mathbf{p}}}), \boldsymbol{\mu}_{\boldsymbol{x}_{\mathbf{p}}}\right) \\ \text{subject to} \quad & \dot{\boldsymbol{\xi}} - \mathbf{f}\left(t, \boldsymbol{\xi}(t), \mathbf{x}_{\mathrm{c}}(t), \boldsymbol{\mu}_{x_{\mathrm{p}}}\right) = \mathbf{0} \\ & \boldsymbol{\xi}_{\min} \le \boldsymbol{\xi} \le \boldsymbol{\xi}_{\max} \end{aligned} \tag{40}$$

The outer loop shares the same objective and takes the optimal control of the inner loop as its control input, $x_{\mathrm{c}*}$. It is constrained by the reliability constraint (as the feasibility constraint) and design variable bounds.

$$\begin{aligned} \min_{\boldsymbol{\mu}_{\boldsymbol{x}_{\mathbf{p}}}} \min \quad & \theta_{\mathrm{HAWT}}\left(t, \boldsymbol{\xi}(t, \boldsymbol{\mu}_{\boldsymbol{x}_{\mathbf{p}}}), \mathbf{x}_{\mathrm{c}*}(t, \boldsymbol{\mu}_{\boldsymbol{x}_{\mathbf{p}}}), \boldsymbol{\mu}_{\boldsymbol{x}_{\mathbf{p}}}\right) \\ \text{subject to} \quad & Pr\left(y_{\mathrm{L}}(t, x_{\mathrm{c}*}, x_{\mathrm{p}}) \le y_{\mathrm{L,max}}\right) \ge \Phi(\beta^t) \\ & \boldsymbol{x}_{\mathbf{p,min}} \le \boldsymbol{x}_{\mathbf{p}} \le \boldsymbol{x}_{\mathbf{p,max}} \end{aligned} \tag{41}$$

where the reliability constraint is solved as a sub-problem, Eq. 38. The dynamics is simulated through numerical ODE solution, where the optimal control trajectory obtained in the inner loop is considered as a time-varying parameter. The state trajectories are compared with their corresponding constraints. The infinity norm of the constraint violation is taken as the limit state. The double-loop RBCD can be represented using a flowchart as shown in Fig. 7. Note that for the double-loop method, the optimal control problem and the reliability assessment problem are solved at each iteration. This should provide the most accurate results for both sub-problems and therefore should require fewer iterations compared to the single-loop and decoupled methods. However, this by no means indicates the lowest total computational cost. For some problems, the computational cost of reliability assessments could be much larger than optimal control due to excessive simulation time; in this case using SLP or SORA methods may be beneficial due to the reduced number of reliability assessments.

3.3 Single-loop RBCD formulation of HAWT

According to the Karush–Kuhn–Tucker (KKT) theorem (Karush 1939), Eq. 38 admits a necessary optimality condition when

$$\nabla G(U) - \lambda \nabla\left(||U|| - \beta^t\right) = 0, \tag{42}$$

where λ is the Lagrange multiplier. The single-loop RBDO replaces the most probable point sub-problem by its optimality condition, or utilizes a sequential linear programming approach, which can significantly reduce the cost of reliability assessment. For RBCD implementation, we may simply replace the MPP by its linear approximation, x_{p}:

$$x_{\mathrm{p}} = \mu_{\mathrm{xp}} + \sigma \beta^t \frac{\sigma \nabla}{G} ||\sigma \nabla G||, \tag{43}$$

where σ is the vector of design variable standard deviations and ∇G are the gradients of the limit state. Since

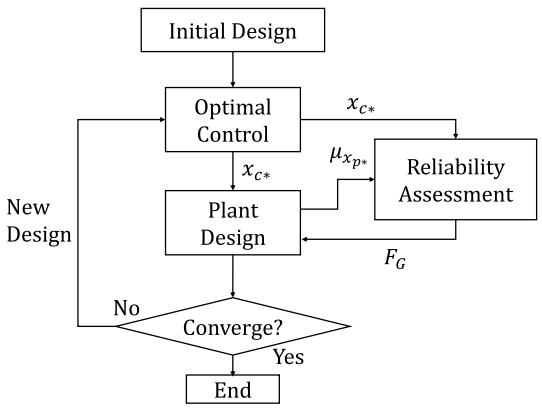

Fig. 7 Reliability-based co-design with double-loop method for reliability assessment

the active constraint, tip deflection, is time-dependent, we may define the limit state as:

$$G\big(t, x_{c*}(t)\big) = max|y_{\mathrm{L}}(t)| - y_{\mathrm{L,max}}, \tag{44}$$

where y_{L} denotes the tip deflection and $y_{\mathrm{L,max}}$ is the upper bound of tip deflection, which is positive. The limit state function here solves the infinity norm of the constraint violation. It is set to zero if the constraint is satisfied. The gradients of the time-dependent limit state are evaluated using a finite difference method, which is also simulation-based and could introduce some additional computational cost.

3.4 Decoupled HAWT RBCD formulation

The double-loop RBDO method requires reliability analysis at each iteration of the outer loop due to its nested formulation, which is accurate but time-consuming. The single-loop method replaces the MPP search sub-problem by its KKT necessary optimality condition, which is very efficient but could fail for maximizing non-concave limit state functions. An alternative is sequential optimization and reliability assessment, or SORA. SORA is one approach to solver RBDO problems in a decoupled manner. Specifically, SORA decomposes the problem into a deterministic design optimization problem with approximated probability constraints and an inverse most probable point problem. The two sub-problems are solved in a sequential manner until convergence. Unlike the double-loop RBDO, SORA only performs reliability analysis once for every completion of the deterministic optimization. This reduces the number of reliability analysis significantly and improves its suitability for solving RBCD problems. The approximation of the reliability constraints in the deterministic design optimization is achieved by introducing a shifting vector:

$$\mathbf{s}_i^{k+1} = \boldsymbol{\mu}_{\mathbf{X}}^{(k)} - \mathbf{X}_{\mathrm{iMPP}}^{(k)}, \tag{45}$$

where $\boldsymbol{\mu}_{\mathbf{X}}^{(k)}$ is the optimal mean design of the deterministic problem in the kth iteration, and $\mathbf{X}_{\mathrm{iMPP}}^{(k)}$ indicates the MPP of the kth iteration. For the corresponding deterministic problem, its constraints are evaluated at the design points after applying the shift, which can be formulated as:

$$\begin{aligned} \min_{\boldsymbol{\mu}_{\mathbf{x_p}}} \quad & \theta_{\mathrm{HAWT}}\Big(t, \boldsymbol{\xi}(t, \boldsymbol{\mu}_{\mathbf{x_p}}), \mathbf{x}_{c*}(t, \boldsymbol{\mu}_{\mathbf{x_p}}), \boldsymbol{\mu}_{\mathbf{x_p}}\Big) \\ \text{subject to} \quad & y_{\mathrm{L}}(t, x_{c*}, \boldsymbol{\mu}_{\mathbf{x}_\mathrm{p}} - \mathbf{s}_i^{k+1}) \le y_{\mathrm{L,max}} \\ & \boldsymbol{x}_{\mathbf{p,min}} \le \boldsymbol{x}_{\mathbf{p}} \le \boldsymbol{x}_{\mathbf{p,max}} \end{aligned} \tag{46}$$

The SORA method is trading the number of iterations to reduce the number of reliability assessments. Therefore, they require high accuracy for both optimal control and reliability assessment for good convergence performance. The method can be represented using a flowchart as shown in Fig. 8.

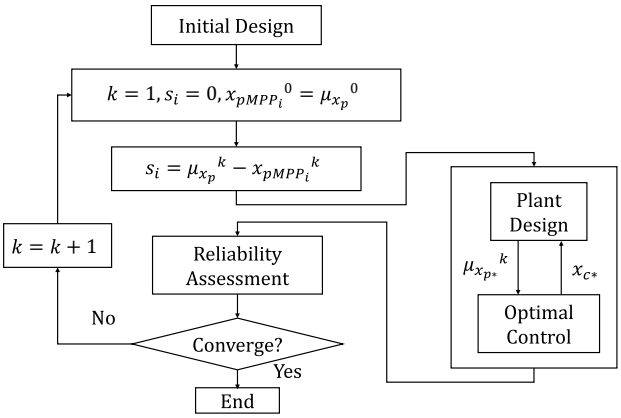

Fig. 8 Reliability-based nested co-design flowchart

The whole procedure starts with an arbitrary choice of initial design with a zero shifting vector. Then it starts the iteration between deterministic co-design with shifting vectors and reliability analysis. The deterministic co-design is a bi-level problem, where the optimal control problem is solved first. The optimal control policy is sent to the outer loop plant design for cost evaluation at non-shifted design points, as well as being sent to the reliability analysis loop for simulation. The detailed steps of this process are as follows:

1. Initialize the plant design $\boldsymbol{\mu}_{\mathbf{x_{p0}}}$. For the common co-design problem formulation, the initial plant design can be identified in the feasible design region where a feasible controller design exists.
2. Within the SORA framework, the RBCD problem is solved iteratively as a nested co-design problem and an inverse reliability assessment problem.
3. For the deterministic co-design problem, solve the optimal control problem for the shifted plant design in the inner loop. The obtained control input is shared with the outer loop plant design, for use in evaluating outer loop cost and constraint components.
4. After convergence of the previous step, the deterministic co-design result for the shifted plant design is used to evaluate the reliability constraints. The reliability constraints are approximated as a shift toward the most probable point. If the reliability constraint is active, the shifted design will touch the limit state, which leads to a control policy that is conservative for the non-shifted design yet is aggressive for the shifted design.
5. The deterministic co-design and reliability assessment sub-problems are solved iteratively until convergence of the most probable point and a feasible non-shifted design.

6. If the design fails to meet the stopping criteria, a new candidate plant design will be proposed by the plant optimizer. Steps 2–4 are then repeated with the updated shifting vector.

The outer loop is solved using `fmincon` using default tolerances, $1e-6$, on constraints, optimality, and numerical convergence. The inner loop optimal control problem is solved using GPOPS–II (Patterson and Rao 2016), which is a commercially available software for solving optimal control problems using collocation and sparse nonlinear programming (NLP) methods. It works by transcribing the infinite-dimensional optimal control problem into a finite-dimension nonlinear program via time discretization of state and control trajectories using global polynomials. The system dynamics constraints ($\mathbf{f}(\cdot)$) are transformed from a system of ordinary differential equations into a set of algebraic constraints when performing this discretization. The method can also be referred to as direct transcription (DT), one class of discretize-then-optimize methods that has proven to be particularly effective for co-design, either for nested or simultaneous formulations. With proper meshing, the co-design problem can be solved accurately and efficiently (Allison and Herber 2014). Some key GPOPS − II parameters are summarized in Table 3.

The control trajectory adds many degrees of freedom, of which the exact number depends on the specific meshing in the time-domain. The solver finds local optima, and the high problem dimension can increase the probability of missing the global optimum or encountering saddle point issues. Solution efficiency is often improved by using the optimal control trajectory of the previous iteration as the initial guess for the current optimal control problem. In the results here we claim only local optimality, and for consistency we use the same initial design and control trajectory for all implemented methods. In practice, different initialization techniques can be applied to improve convergence performance.

Table 3 GPOPS − II settings

Field	Setting
Mesh method	hp–LiuRao–Legendre
Mesh tolerance	10^{-3}
NLP solver	IPOPT
Linear solver	ma57
IPOPT tolerance	10^{-11}
IPOPT max iteration number	100
Derivative supplier	sparseFD
Derivative level	Second

Another note is that sometimes a hard limit on the maximum number of iterations on the inner loop optimal control is placed to account for cases when optimal control problem takes an impractical amount of time to solve. For the wind turbine problem, it was found that a poor guess of initial control requires approximately 40–50 iterations to converge to a feasible result. This is reduced to about 20 iterations when an optimal control trajectory from the previous iteration is used as the initial guess. Any inner loop problem that requires more than 100 iterations is stopped by the optimal control solver. If a properly chosen feasibility constraint is present in the outer loop, the overall co-design algorithm will still find a feasible design and control combination. This can be considered as a potential advantage of nested co-design over the simultaneous formulation, which allows the inner loop to stop prematurely for efficiency yet still converge to a feasible solution.

4 Results

In this section, we present the results of deterministic and reliability-based co-design. To explore the tradeoff between energy production and tower mass a parametric multi-objective solution strategy was employed, and the resulting Pareto fronts are presented as the major results, along with their specific optimal design and corresponding state and control trajectories. The common initial design is specified as $\boldsymbol{x}_{\mathbf{p}} = [80, 200, 10, 9.9]$, which is the most conservative design within the design space. A conservative initial tower design guarantees the existence of an optimal control solution in the inner loop; i.e., the co-design problem is initialized within the feasible design space.

As shown in Fig. 9, the energy production increases with increasing allowed tower mass, with a steep gradient in the low-mass region and flatter gradient in the heavier tower region. All reliability-based co-design solutions converge to a more conservative tower design compared to deterministic

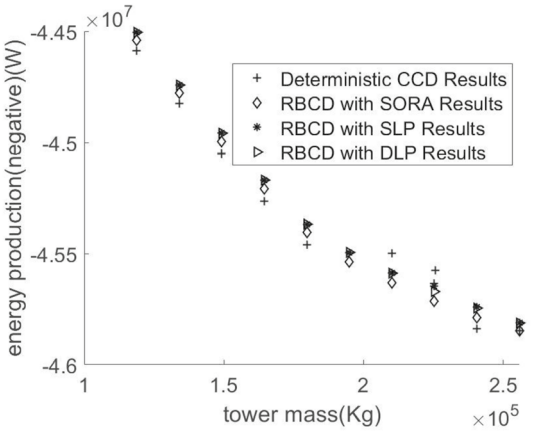

Fig. 9 HAWT CCD and RBCD pareto frontiers of the HAWT

solutions, and therefore result in lower energy production, or higher levelized cost of energy. Also, the fact that the three RBCD strategies converge to the same Pareto front indicates the efficacy, and validate the robustness of the model and problem formulation across the different RBDO methods.

We consider the deterministic co-design results, summarized in Table 4, as the benchmark. The height of the tower, L, serves as the main coupling factor as its derivative with respect to the optimal power production is steady. This agrees with the wind model that wind speed is higher at greater altitude. The width and thickness of the tower are critical for the structural stability, that they reach the upper bound quickly as the tower mass increases. The tapper ratio of the tower is the least sensitive design parameter; it only becomes influential as the width and thickness reach their upper bounds. For the 10th point on the Pareto front, which represents a case that the tower weight is at its maximum or over-design, the optimal tower width and thickness actually dropped. The structural stability is compensated by a drastic increase in the tapper ratio. The over-designed 10th tower also resulted in a large drop in the probability of failure as compared with towers 1–9; however, it is still above the target, 5%. Note that the probability of failure does not necessarily drops as the weight of the tower increases, since a more aggressive control strategy may be adopted by inner loop.

The probability of failure (POF) is validated using a Monte Carlo Simulation (MCS) with a sample size of 10^4. We observe a continuous drop of POF as we increase the tower weight, such that the extra material can be allocated to increase the strength of the tower. For an over-designed tower, the 10*th* tower, there is a significant drop in the POF. This also shows that over-design can be less effective for design problems with uncertainties compared to explicit treatment of reliability.

The RBCD results obtained from the double-loop method (as shown in Table 5), the single-loop method (as shown in Table 6), and SORA (as shown in Table 7) are very close. Comparing against the benchmark results, the optimal designs have lower heights to reduce the load on the towers, and wider and thicker towers for enhanced strength. These conservative designs leave less space for the tapper ratio, so we observe a lower gradients of tower tapper ratio for heavy tower designs. All the RBCD implementations result in feasible solutions regarding the reliability constraint, which is 95%. They show trends similar to the deterministic co-design results, where the POF decreases as the tower weight increases.

Among the three RBCD implementations, the SORA-based method requires the lowest number of iterations. All points on the Pareto front converged within three iterations. The double-loop and single-loop methods have similar

Table 4 Design results of the deterministic pareto front

Index	L_1 (m)	L (m)	d_1 (m)	d_{1i} (m)	$\frac{dL_{1*}}{dObj_*}$	$\frac{dL_*}{dObj_*}$	$\frac{dd_*}{dObj_*}$	$\frac{dd_{i*}}{dObj_*}$	POF (%)
1	200.16	87.34	7.17	7.16	0	0.07	0.01	0.01	45.49
2	200.16	93.33	7.83	7.82	0	0.07	0.01	0.01	45.44
3	200.16	98.96	8.49	8.48	0	0.07	0.01	0.01	45.29
4	200.16	104.44	9.14	9.13	0	0.07	0.01	0.01	45.21
5	200.16	109.74	9.80	9.79	0.12	0.08	0.01	0.01	45.17
6	214.15	113.60	10.06	10.05	0.47	0.08	0	0	45.07
7	239.56	116.35	10.06	10.05	0.84	0.08	0	0	45.04
8	268.40	118.84	10.06	10.05	1.08	0.08	0	0	44.97
9	301.57	121.10	10.06	10.05	2.93	0.08	0	0	45.89
10	353.25	121.26	10.01	10.00	27.73	0.08	− 0.03	− 0.03	15.56

Table 5 Design results of the DLP-based RBCD pareto front

Index	L_1 (m)	L (m)	d_1 (m)	d_{1i} (m)	$\frac{dL_{1*}}{dObj_*}$	$\frac{dL_*}{dObj_*}$	$\frac{dd_*}{dObj_*}$	$\frac{dd_{i*}}{dObj_*}$	*Iter*	*Obj*	RA	POF (%)
1	200.16	85.43	7.25	7.24	0	0.07	0.01	0.01	6	6	6	4.81
2	200.16	91.33	7.91	7.90	0	0.07	0.01	0.01	5	5	5	4.83
3	200.16	96.84	8.57	8.56	0	0.07	0.01	0.01	6	6	6	4.82
4	200.16	102.19	9.23	9.22	0	0.07	0.01	0.01	6	6	6	4.76
5	200.16	107.38	9.88	9.87	0.15	0.07	0.01	0.01	9	9	9	4.74
6	217.69	110.88	10.06	10.05	0.56	0.08	0	0	11	11	11	4.74
7	244.58	113.55	10.06	10.05	0.91	0.08	0	0	12	13	13	4.73
8	275.40	115.96	10.06	10.05	1.18	0.08	0	0	11	12	12	4.69
9	311.30	118.15	10.06	10.05	1.54	0.08	0	0	10	10	10	4.71
10	353.86	120.16	10.06	10.05	1.76	0.08	0	0	8	11	11	4.71

Table 6 Design results of the SLP-based RBCD Pareto Front

Index	L_1 (m)	L (m)	d_1 (m)	d_{1i} (m)	$\frac{dL_{1*}}{dObj_*}$	$\frac{dL_*}{dObj_*}$	$\frac{dd_*}{dObj_*}$	$\frac{dd_{i*}}{dObj_*}$	*Iter*	*Obj*	*RA*	POF (%)
1	200.16	85.43	7.25	7.24	0	0.07	0.01	0.01	6	7	7	4.81
2	200.16	91.33	7.91	7.90	0	0.07	0.01	0.01	5	5	5	4.83
3	200.16	96.84	8.57	8.56	0	0.07	0.01	0.01	5	5	5	4.83
4	200.16	102.19	9.23	9.22	0	0.07	0.01	0.01	5	5	5	4.76
5	200.16	107.38	9.88	9.87	0.15	0.07	0.01	0.01	6	6	6	4.77
6	217.69	110.89	10.06	10.05	0.56	0.08	0	0	8	12	12	4.77
7	244.57	113.55	10.06	10.05	1.30	0.08	0	0	9	14	14	4.74
8	288.38	115.21	9.88	9.87	0.95	0.08	0	0	6	21	21	4.69
8*	275.40	115.96	10.06	10.05	–	–	–	–	9	9	9	4.71
9	297.44	118.06	10.06	10.05	1.09	0.08	0	0	15	60	60	4.68
9*	311.30	118.15	10.06	10.05	–	–	–	–	9	12	12	4.73
10	353.85	120.17	10.06	10.05	2.22	0.08	0	0	11	15	15	4.73

Table 7 Design results of the SORA-based RBCD pareto front

Index	L_1 (m)	L (m)	d_1 (m)	d_{1i} (m)	$\frac{dL_{1*}}{dObj_*}$	$\frac{dL_*}{dObj_*}$	$\frac{dd_*}{dObj_*}$	$\frac{dd_{i*}}{dObj_*}$	*Iter*	*Obj*	*RA*	POF (%)
1	200.16	85.43	7.25	7.24	0	0.07	0.01	0.01	3	12	3	4.81
2	200.16	91.33	7.91	7.90	0	0.07	0.01	0.01	3	12	3	4.83
3	200.16	96.84	8.57	8.56	0	0.07	0.01	0.01	3	13	3	4.82
4	200.16	102.19	9.23	9.22	0	0.07	0.01	0.01	3	13	3	4.76
5	200.16	107.38	9.88	9.87	0.15	0.07	0.01	0.01	3	15	3	4.74
6	217.69	110.88	10.06	10.05	0.56	0.08	0	0	3	15	3	4.74
7	244.58	113.55	10.06	10.05	0.91	0.08	0	0	3	18	3	4.73
8	275.40	115.96	10.06	10.05	1.18	0.08	0	0	3	20	3	4.69
9	311.30	118.15	10.06	10.05	1.54	0.08	0	0	3	20	3	4.71
10	353.86	120.16	10.06	10.05	1.76	0.08	0	0	3	19	3	4.71

iteration counts, with the caveat that more iterations are needed for heavier towers. One potential cause of such a scenario is that heavier towers are more likely to be feasible, which yield smaller gradients for the constraint violation. In fact, the 8*th* and 9*th* point on the SLP Pareto front terminated at points that did not satisfy optimality criteria to the specified tolerance. MCS tests, however, showed that these two designs are still feasible. Also, convergence behavior can be improved by adjusting the step size of the finite difference method used to approximate the limit state function gradients (i.e., from 1e-6 to 1e-3). This suggests that the SLP method is more sensitive to gradients information, which is reasonable since it depends on this information for the linearized KKT condition. If we take a closer look at the total number of optimal control and reliability assessments, we see that SORA is in fact shifting the computational cost from the reliability assessment to optimal control. Again, the SORA implementation only evaluate the reliability after each convergence of a shifted deterministic co-design problem; consequently, the total number of reliability assessment will be significantly reduced if the total number of iterations is low. However, the total number of optimal control sub-problem solutions is much larger than for the other RBCD implementations.

As identified above, tip deflection is the only active reliability constraint in this problem. It is reasonable to move forward assuming that this constraint is active because 1) it was found to be the only active constraint of the inner loop optimal control problem, 2) it is directly coupled with the wind load and the design variables, and 3) early investigations showed that this constraint was consistently active. To validate such assumption and formulation simplification, we performed MCS of size 10^3 for point 1, 5, and 10 using each RBCD method; these tests represent solution behavior for heavy, medium, and light-weight towers. The results are summarized in Table 8.

The minimum and maximum value of the MCS state trajectories are all within the lower and upper state bounds. This suggests that the uncertainty-induced variation in states is not large enough to turn inactive constraints active, tip deflection (upper bound) is indeed the only active reliability constraint. Therefore, the formulation simplification is valid for this wind turbine RBCD problem. However, this simplification is based on a good understanding of the uncertainty and its quantitative effects on the dynamics. In a general case, or if such knowledge is lacking, all the states and path constraints may need to be treated as reliability constraints.

Table 8 In-activeness of other sate constraints under uncertainty

Index	Q (MN · m)	T (MN)	ω (rad/s)	Ω (rad/s)	ϕ (rad)	M_{gen} (KN · m)
LB, UB	0, 5	0, 0.5	1.26, 1.51	122.52, 146.61	− 0.0175, 0.0175	0, 47.40
DLP 1	0.03, 0.38	0.11, 0.40	1.28, 1.47	124.39, 142.74	0.0004, 0.0062	35.16, 38.70
DLP 5	0.05, 0.42	0.13, 0.43	1.32, 1.47	127.54, 142.70	0.0006, 0.006	35.16, 37.37
DLP 10	0.06, 0.43	0.13, 0.44	1.33, 1.47	128.44, 142.69	0.0007, 0.0059	35.16, 37.05
SLP 1	0.03, 0.38	0.11, 0.40	1.28, 1.47	124.39, 142.74	0.0004, 0.0062	35.16, 38.70
SLP 5	0.05, 0.42	0.13, 0.43	1.32, 1.47	127.54, 142.70	0.0006, 0.006	35.16, 37.37
SLP 10	0.06, 0.43	0.13, 0.44	1.33, 1.47	128.44, 142.69	0.0007, 0.0059	35.16, 37.05
SORA 1	0.03, 0.38	0.11, 0.40	1.28, 1.47	124.39, 142.74	0.0004, 0.0062	35.16, 38.70
SORA 5	0.05, 0.42	0.13, 0.43	1.32, 1.47	127.54, 142.70	0.0006, 0.006	35.16, 37.37
SORA 10	0.06, 0.43	00.13, 0.44	1.33, 1.47	128.44, 142.69	0.0007, 0.0059	35.16, 37.05

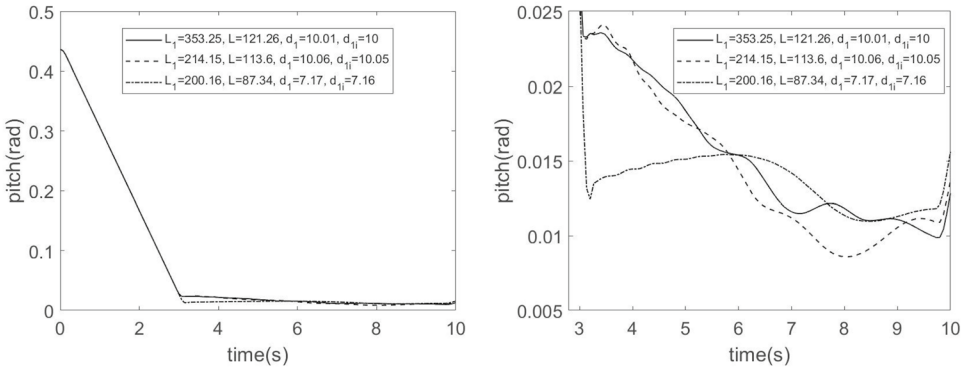

(a) Pitch Angle **(b)** Pitch Angle (zoom-in)

Fig. 10 Control trajectories of HAWT deterministic co-design

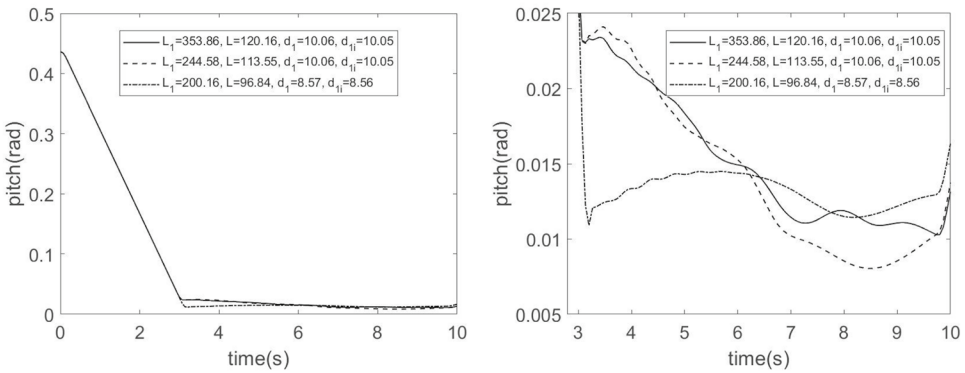

(a) Pitch Angle **(b)** Pitch Angle (zoom-in)

Fig. 11 Control trajectories of HAWT Reliability-based co-design with DLP

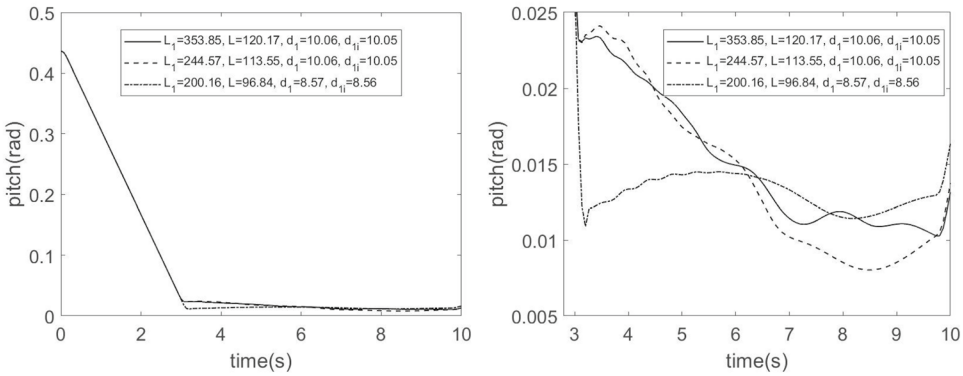

(a) Pitch Angle **(b)** Pitch Angle (zoom-in)

Fig. 12 Control trajectories of HAWT reliability-based co-design with SLP

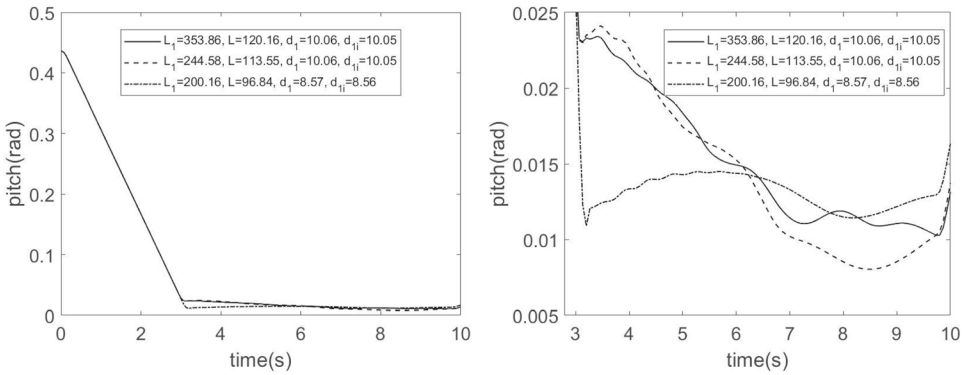

(a) Pitch Angle **(b)** Pitch Angle (zoom-in)

Fig. 13 Control trajectories of HAWT reliability-based co-design with SORA

We can also inspect the optimal control trajectories. For the pitch-controlled rotor blade, a lower pitch angle lead to a larger thrust load, given the same wind velocity and angular velocity. On the same Pareto front, the heavier towers allow the rotor to spin at a faster speed for their faster wind speeds. However, they compensate the increased load by choosing more conservative pitch angles. In the contrast, lighter lower-elevation towers are subject to slower wind speeds, so they reduce the angular velocity of the rotor and choose a more aggressive pitch trajectory. This is a result from the effect of balancing between the power output and thrust load, a core design coupling mechanism in this CCD problem (Figs. 10, 11, 12, 13).

The details of the state and control trajectories at the optimum HAWT designs obtained using the deterministic co-design and RBCD problem formulations have been provided in "Appendices 2" to "Appendices 5". Comparing the control trajectories between the RBCD and its deterministic benchmark, the RBCD control trajectories for light towers are slightly more aggressive. This can serve as an evidence of the design coupling between the plant design and the control design, specifically, that the conservativeness of one sub-system will affect the optimal solution of the other. Further studies with quantitative evaluations of such coupling effects can help to reveal greater insights into this design relationship.

5 Conclusion

In this work, the uncertainty-based HAWT co-design problem is decomposed into a nested problem involving plant design, a robust optimal control trajectory design, and reliability assessment. The nested co-design structure supports intuitive strategies for updating the plant design as well as the corresponding dynamics. It also enables more efficient allocation of computational design burdens across plant and control design sub-problems. State-of-art co-design

strategy primarily utilize OLC strategies to enhance comprehensive plant design exploration. This characteristic places no limitation on the specific control strategy and certainly does not admits consideration of advanced control strategies.

The current formulation considers different types of uncertainties, which includes loading uncertainties and model uncertainties. Loading cases are generated following the spatial and statistical distribution, which are characterized from actual wind data and can be generated for arbitrary numbers of test cases. All the generated wind profiles follow the site-specific Weibull distribution. The parametric uncertainty is integrated using double-loop, single-loop, and SORA. With proper formulation, all three RBDO methods can be utilized in solving the CCD problem. Results show the efficacy as well as offer a flavor of how different algorithms allocate the computational cost. These results provide insights that may help in choosing appropriate RBCD methods for different engineering problems, especially when there is a significant difference in computational cost between the optimal control problem and the reliability assessment problem.

We introduced multidisciplinary dynamic models of a HAWT that has been tailored for co-design and RBCD implementations. The aerodynamics of the rotor and the structural dynamics of the tower can be updated conveniently without any extra simulations or surrogate modeling. Transmission and generator system design are assumed to be fixed, so they are only modeled using simplified dynamics. By selecting appropriate models, we can solve multidisciplinary dynamic problems efficiently yet still capture their coupling effects.

For future work, an accurate and efficient estimation of the robustness term in the relaxed nested structure should be investigated. In addition, an efficient reliability estimation for path constraints would help to reduce the computational cost for the design of dynamic systems.

Appendices

Appendix 1: NREL 5MW wind turbine blade parameters

This appendix provides the NREL 5MW wind turbine blade parameters (Jager and Andreas 1996). Additionally, the listed airfoils are corresponding to the lift and drag coefficients extended to $[-180°, 180°]$, based on the DOWEC blades (Kooijman et al. 2003; Lindenburg 2002) (Table 9).

Table 9 NREL 5MW wind turbine blade element properties

Element	r (m)	Pre-bent angle (°)	dr (m)	c (m)	Airfoil
1	2.8667	13.308	2.7333	3.542	Cylinder1
2	5.6000	13.308	2.7333	3.854	Cylinder1
3	8.3333	13.308	2.7333	4.167	Cylinder2
4	11.7500	13.308	4.1000	4.557	DU40_A17
5	15.8500	11.480	4.1000	4.652	DU35_A17
6	19.9500	10.162	4.1000	4.458	DU35_A17
7	24.0500	9.011	4.1000	4.249	DU30_A17
8	28.1500	7.795	4.1000	4.007	DU25_A17
9	32.2500	6.544	4.1000	3.748	DU25_A17
10	36.3500	5.361	4.1000	3.502	DU21_A17
11	40.4500	4.188	4.1000	3.256	DU21_A17
12	44.5500	3.125	4.1000	3.010	NACA64_A17
13	48.6500	2.319	4.1000	2.764	NACA64_A17
14	52.7500	1.526	4.1000	2.518	NACA64_A17
15	56.1667	0.863	2.7333	2.313	NACA64_A17
16	58.9000	0.370	2.7333	2.086	NACA64_A17
17	61.6333	0.106	2.7333	1.419	NACA64_A17

Appendix 2: HAWT deterministic co-design state and control trajectories

Appendix 2 provides state and control trajectories of the optimum design obtained from the HAWT deterministic co-design formulation.

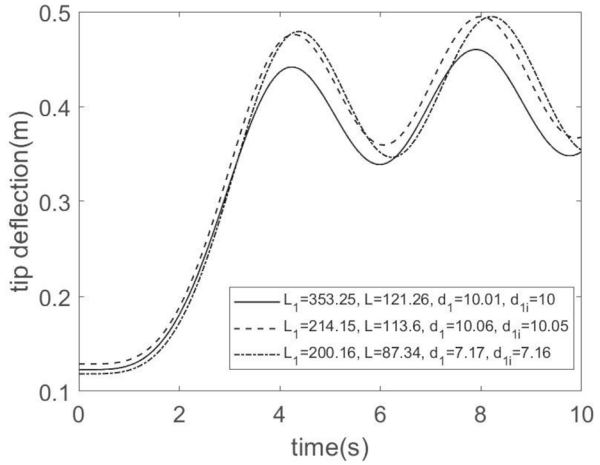

(a) Tip Deflection

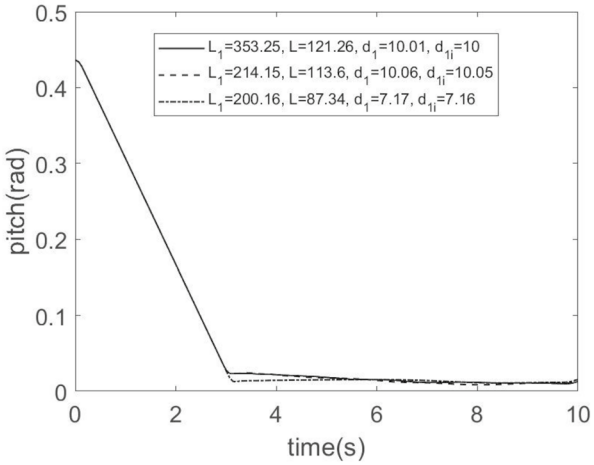

(b) Pitch Angle

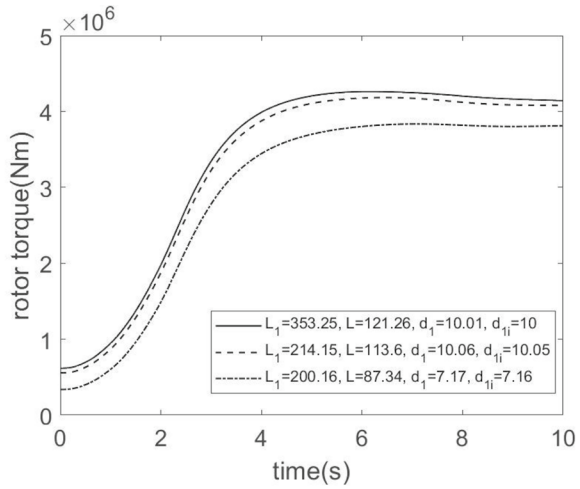

(c) Rotor Torque

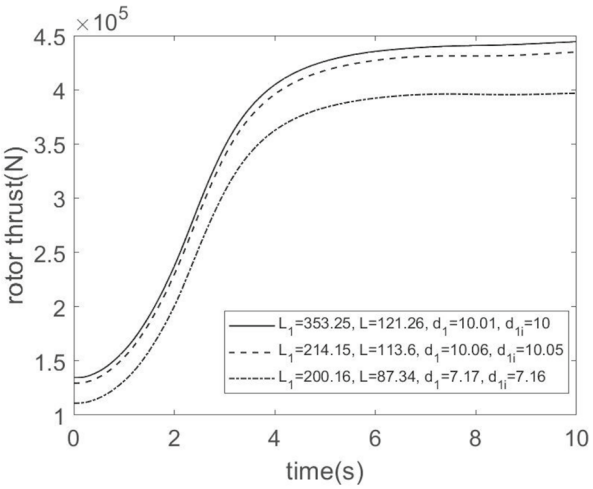

(d) Thrust Force

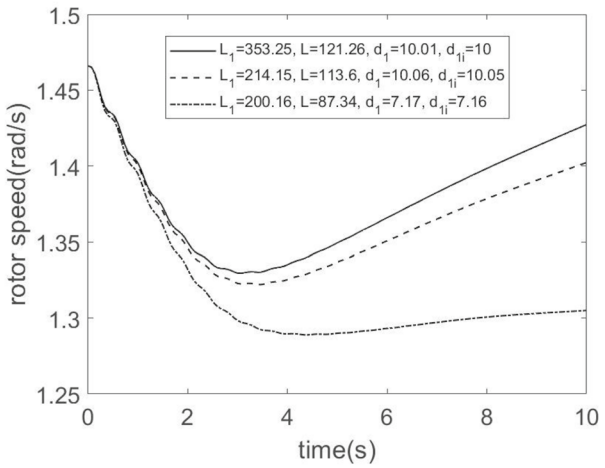

(e) Rotor Velocity

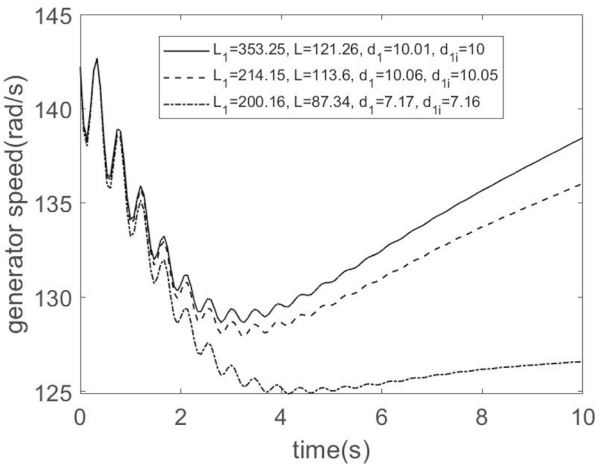

(f) Generator Speed

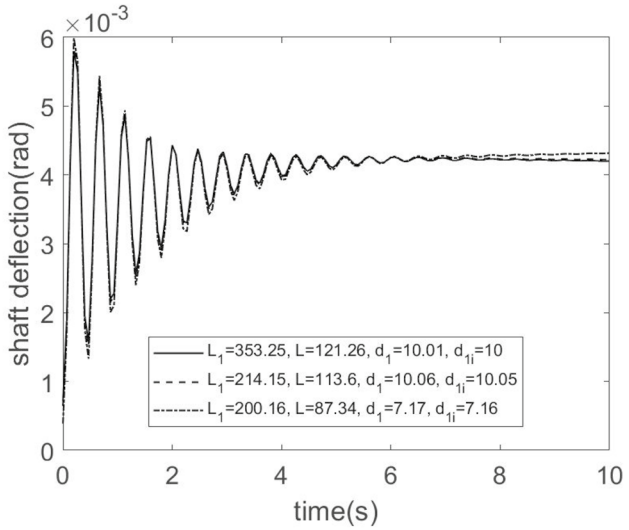

(g) Shaft Deflection

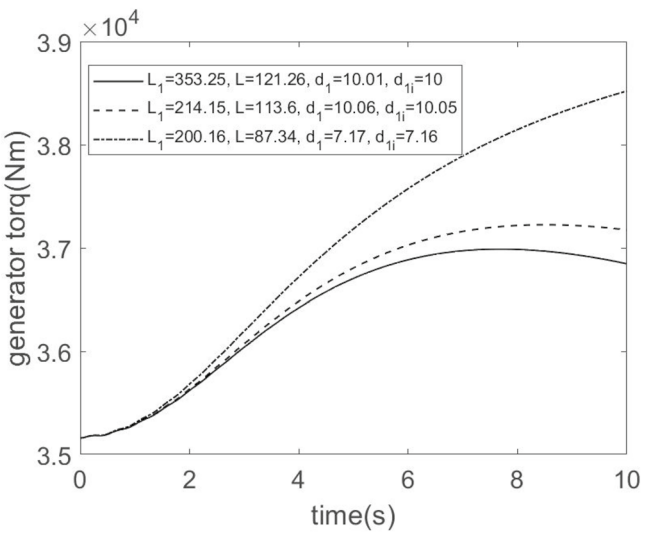

(h) Generator Torque

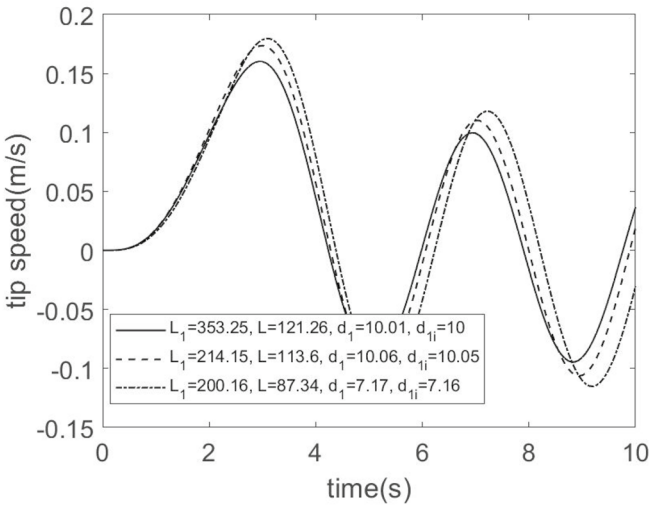

(i) Tip Speed

Appendix 3: HAWT reliability-based co-design with DLP state and control trajectories

Appendix 3 provides state and control trajectories of the optimum design obtained from the HAWT reliability-based co-design with the DLP formulation.

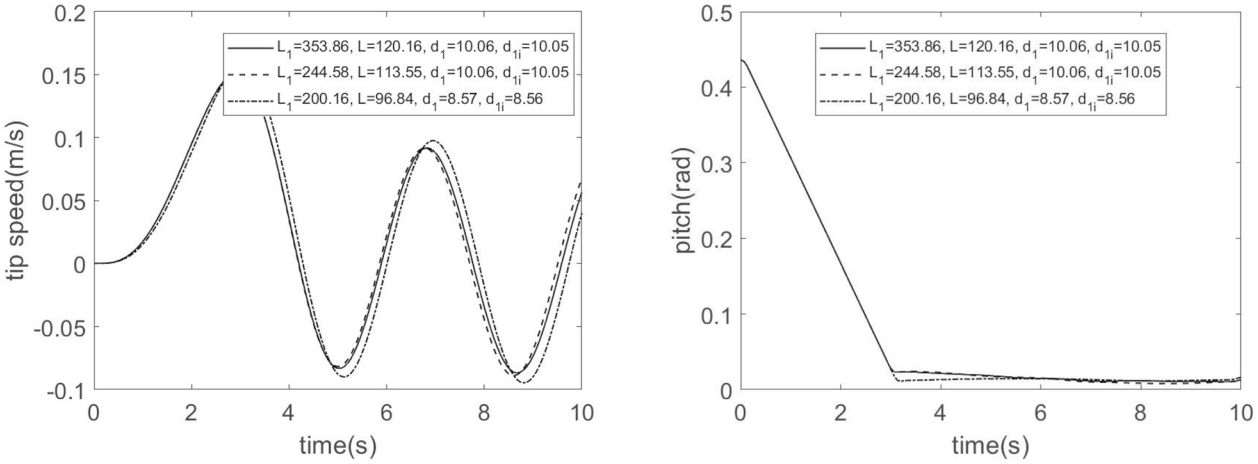

(a) Tip Deflection

(b) Pitch Angle

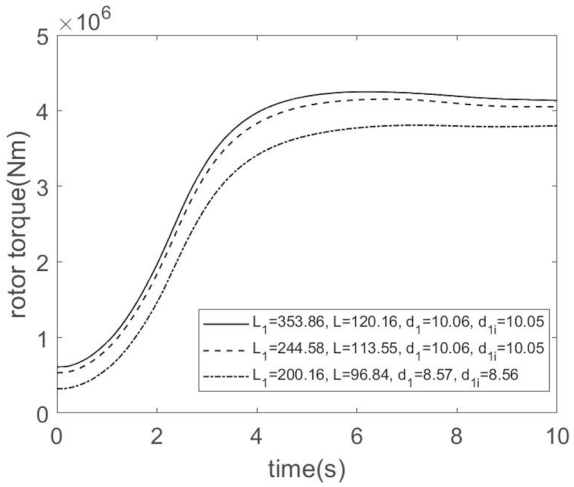

(c) Rotor Torque

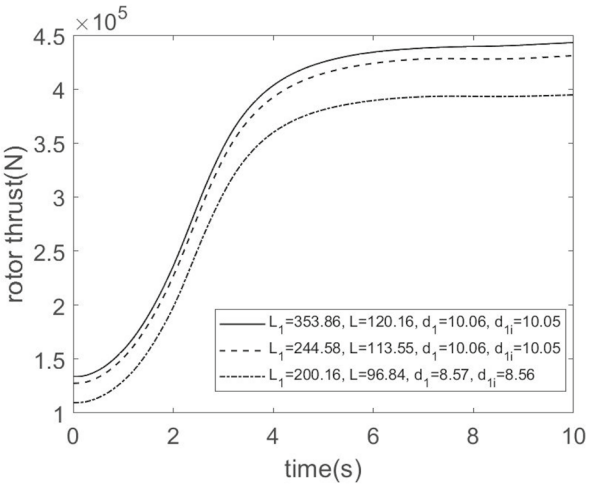

(d) Thrust Force

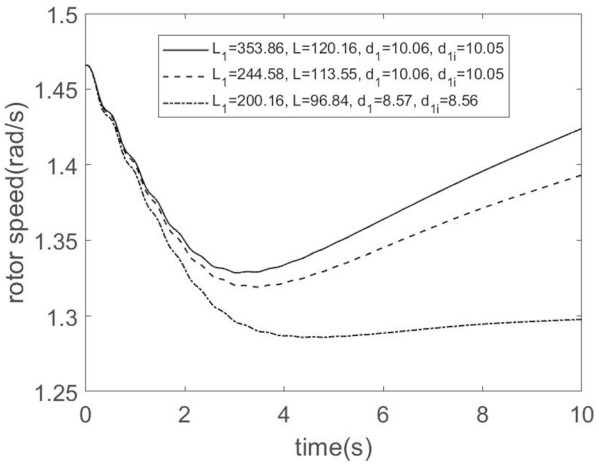

(e) Rotor Velocity

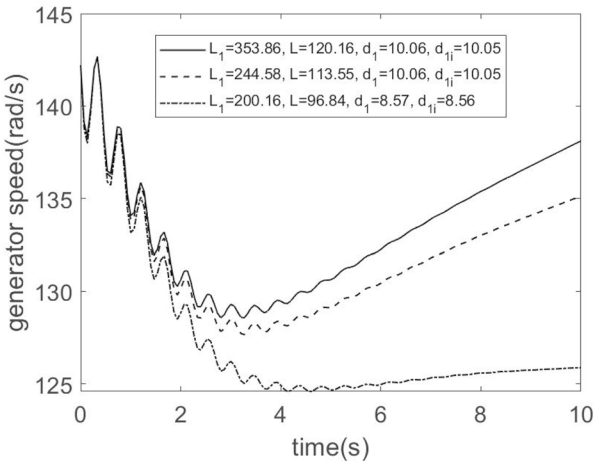

(f) Generator Speed

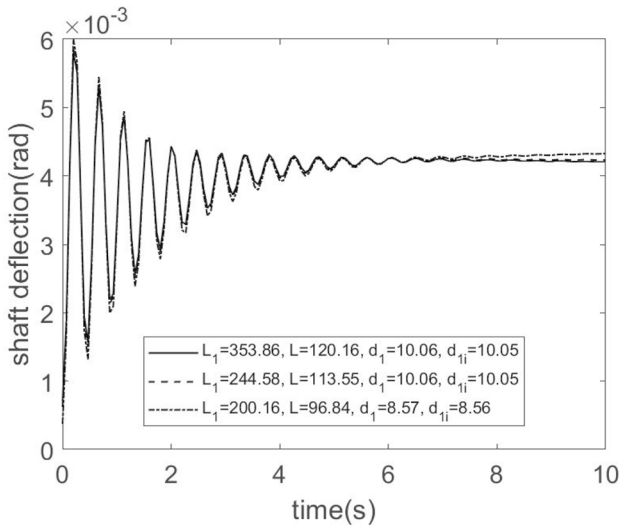

(g) Shaft Deflection

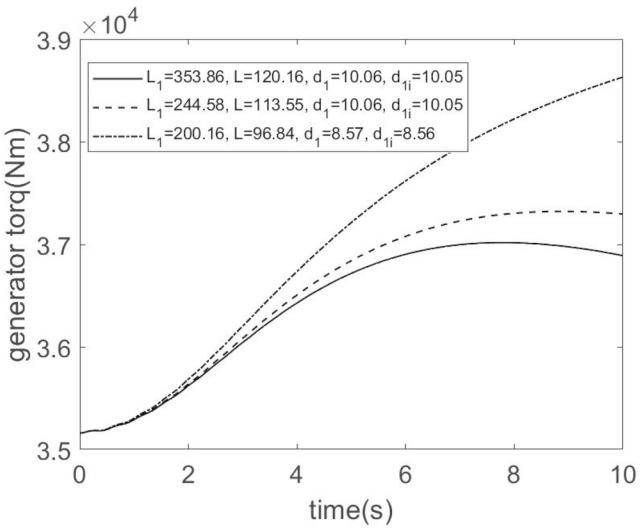

(h) Generator Torque

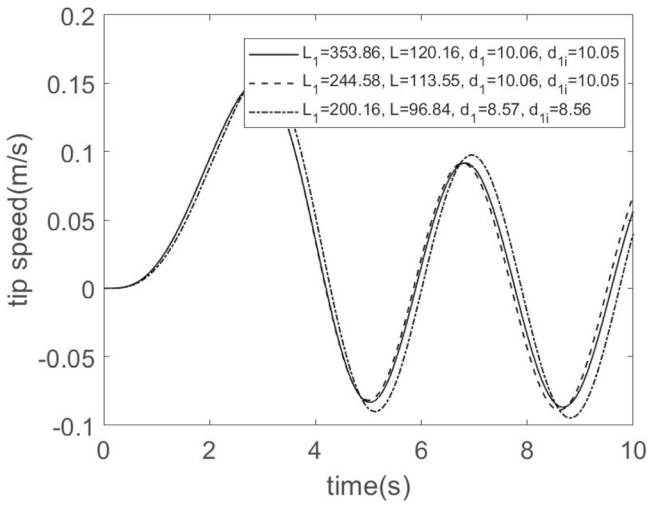

(i) Tip Speed

Appendix 4: HAWT reliability-based co-design with SLP state and control trajectories

Appendix 4 provides state and control trajectories of the optimum design obtained from the HAWT reliability-based co-design with the SLP formulation.

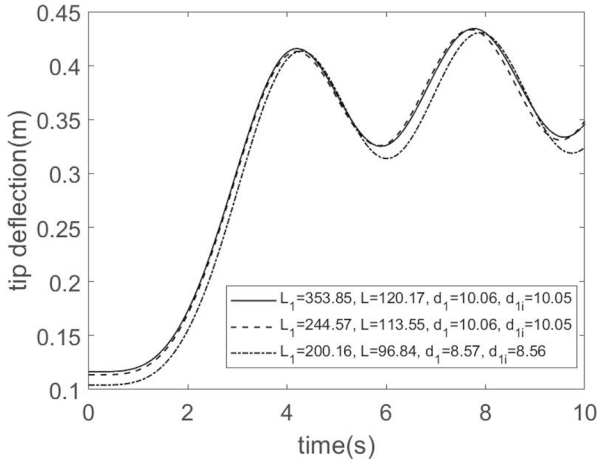

(a) Tip Deflection

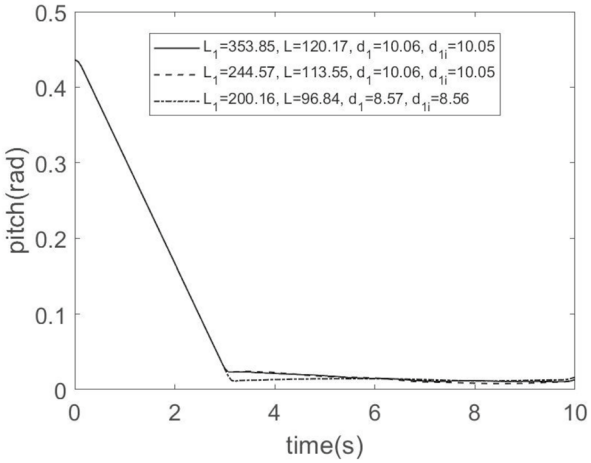

(b) Pitch Angle

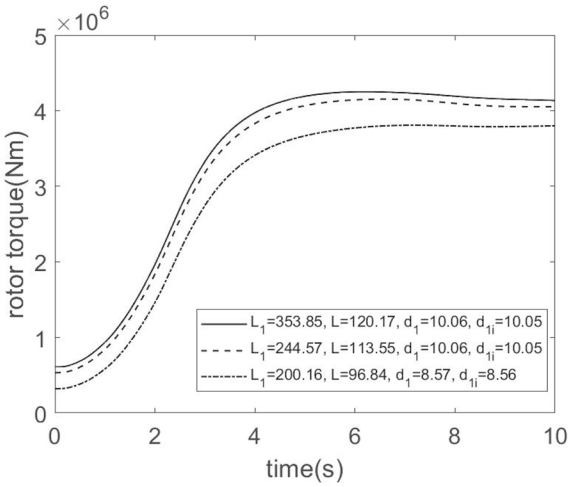

(c) Rotor Torque

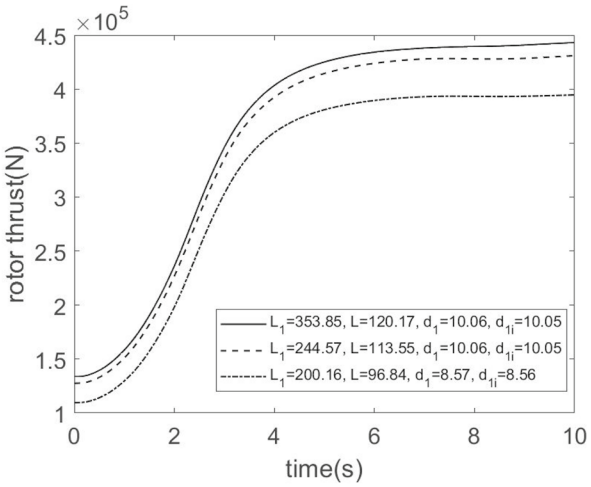

(d) Thrust Force

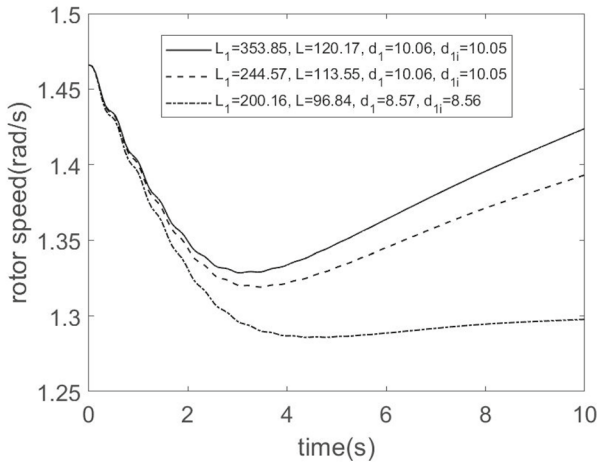

(e) Rotor Velocity

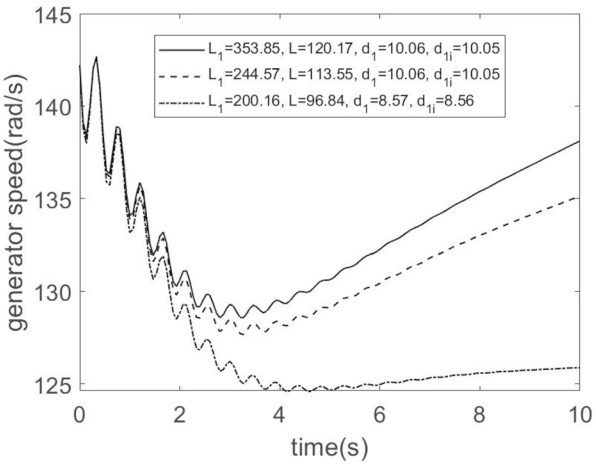

(f) Generator Speed

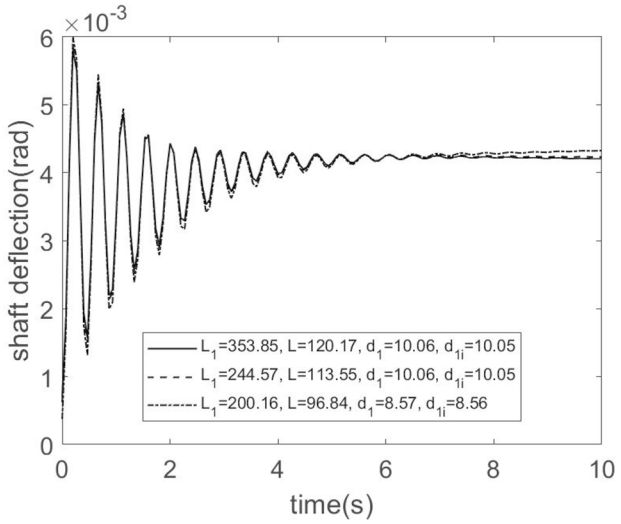

(g) Shaft Deflection

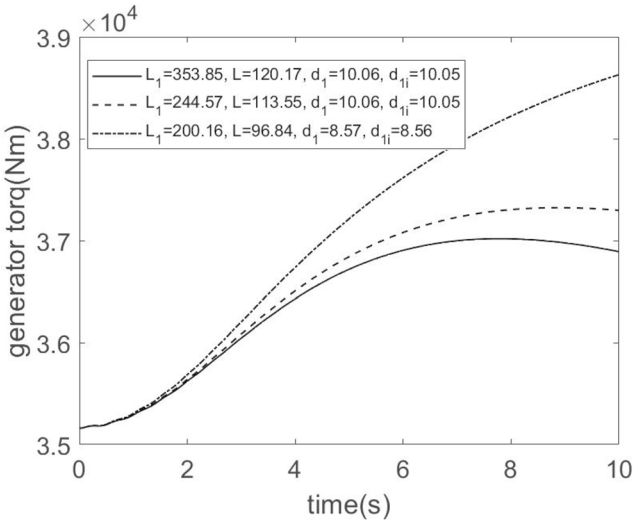

(h) Generator Torque

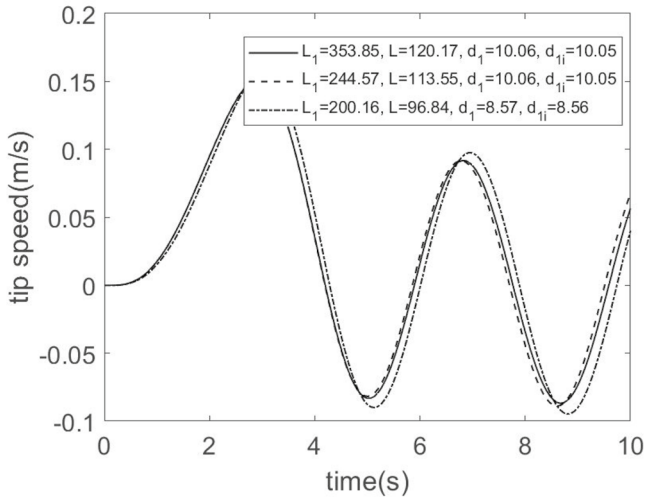

(i) Tip Speed

Appendix 5: HAWT reliability-based co-design with SORA state and control trajectories

Appendix 5 provides state and control trajectories of the optimum design obtained from the HAWT reliability-based co-design with the SORA formulation.

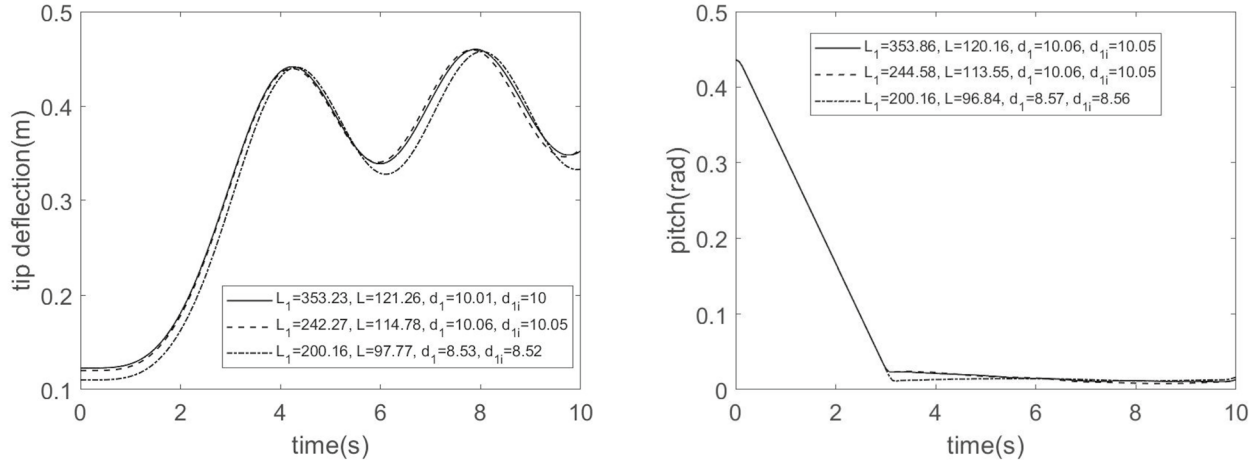

(a) Tip Deflection

(b) Pitch Angle

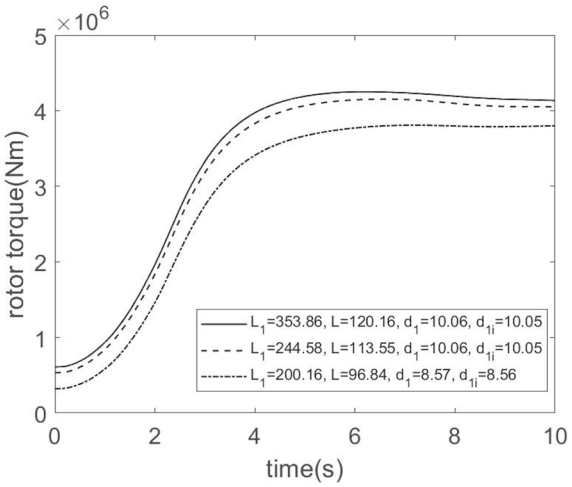

(c) Rotor Torque

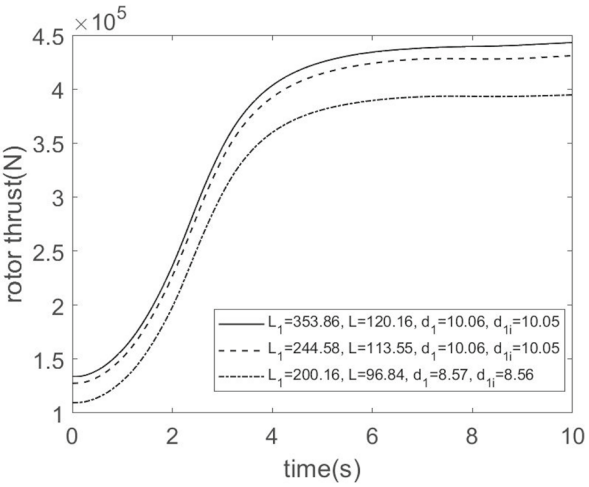

(d) Thrust Force

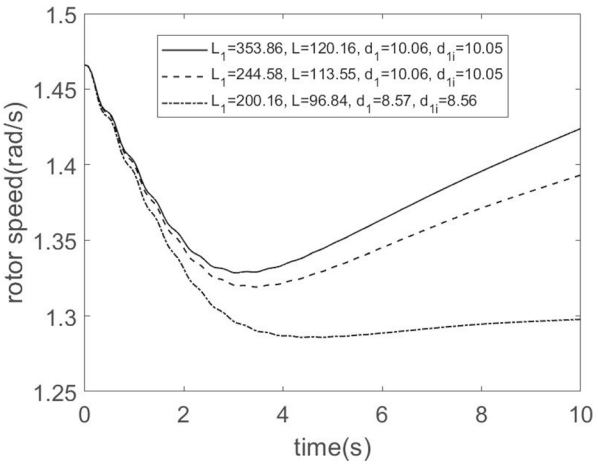

(e) Rotor Velocity

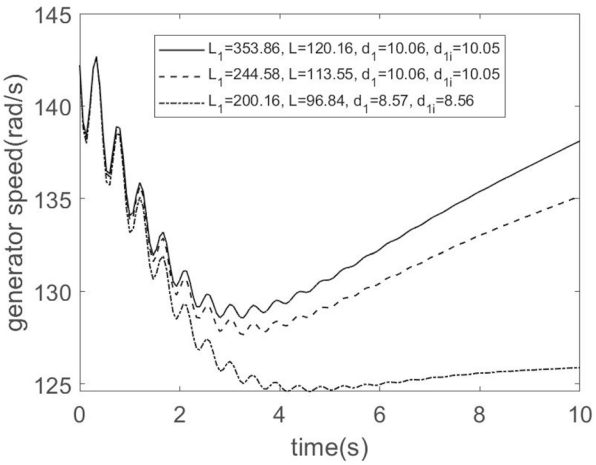

(f) Generator Speed

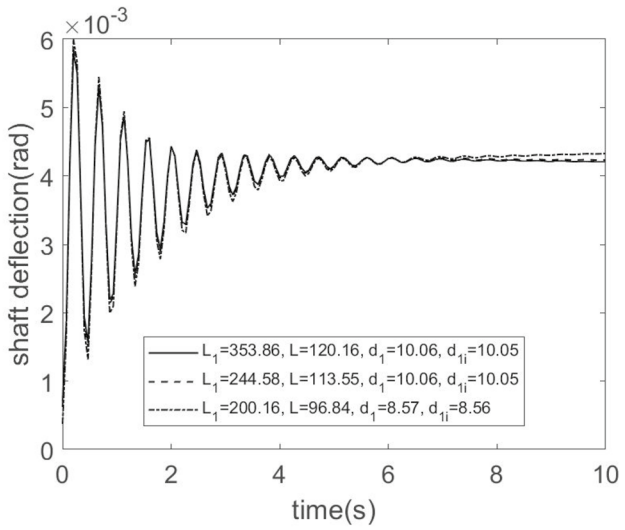

(g) Shaft Deflection

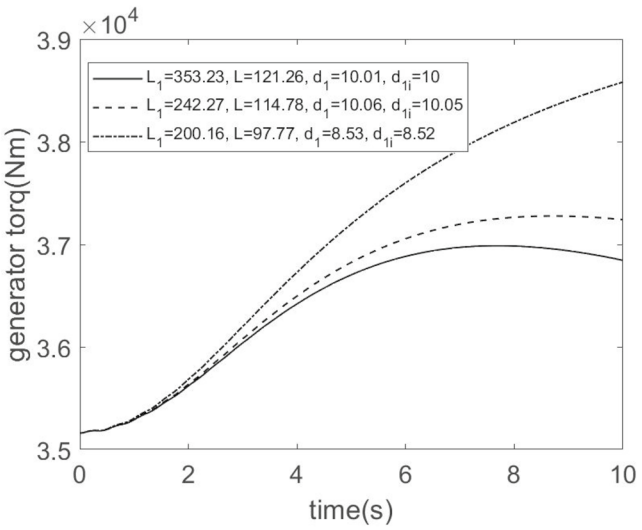

(h) Generator Torque

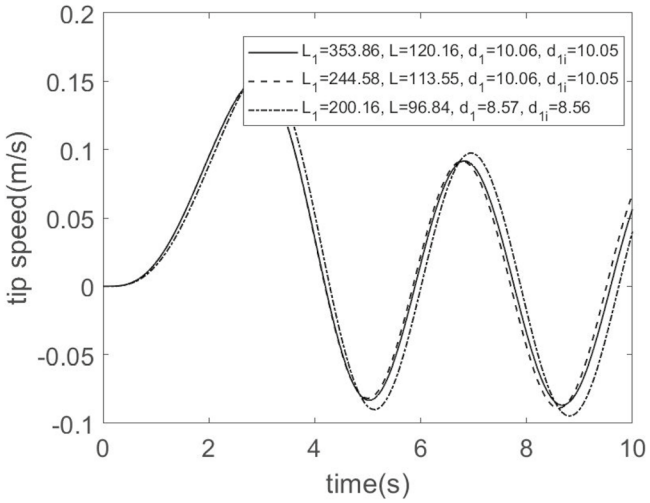

(i) Tip Speed

Acknowledgements This research is partially supported by National Science Foundation through Faculty Early Career Development (CAREER) awards CMMI-1813111 and the Engineering Research Center for Power Optimization of Electro-Thermal Systems (POETS) with cooperative agreement EEC-1449548.

Author contribution All authors have participated in (a) conception and design, or analysis and interpretation of the data; (b) drafting the article or revising it critically for important intellectual content; and (c) approval of the final version.

Declarations

Conflict of interest The authors have affiliations with organizations with direct or indirect financial interest in the subject matter discussed in the manuscript.

Replication of results This manuscript is self-contained, in that it contains all necessary theory and data to reproduce the results, including the preliminaries, i.e., the wind turbine design specifications and the theory on reliability-based co-design methodology. The design problem formulation and all parameters for the examples are provided and described in detail. Lastly, the source codes for the implementation of the wind turbine design study can be provided upon requests from interested readers.

References

Allison JT (2013) Plant-limited co-design of an energy-efficient counterbalanced robotic manipulator. ASME J Mech Des 135(10):101003

Allison JT, Herber DR (2014) Multidisciplinary design optimization of dynamic engineering systems. AIAA J 52(4):691–710

Allison JT, Nazari S (2010) Combined plant and controller design using decomposition-based design optimization and the minimum principle. In: International design engineering technical

conferences and computers and information in engineering conference, vol 44090, pp 765–774
Allison JT, Guo T, Han Z (2014) Co-design of an active suspension using simultaneous dynamic optimization. ASME J Mech Des 136(8):081003
Ashuri T, Zaaijer MB, Martins JR, Zhang J (2016) Multidisciplinary design optimization of large wind turbines—technical, economic, and design challenges. Energy Convers Manag 123:56–70
Azad S, Alexander-Ramos MJ (2020) A single-loop reliability-based MDSDO formulation for combined design and control optimization of stochastic dynamic systems. J Mech Des 143(2):021703
Box GE, Jenkins GM (1970) Time series analysis: forecasting and control Holden-day. San Francisco, p 498
Chiralaksanakul A, Mahadevan S (2005) First-order approximation methods in reliability-based design optimization. ASME J Mech Des 127(5):851–857
Cui T, Allison JT, Wang P (2020a) A comparative study of formulations and algorithms for reliability-based co-design problems. J Mech Des 142(3):031104
Cui T, Allison JT, Wang P (2020b) Reliability-based co-design of state-constrained stochastic dynamical systems. In: AIAA Scitech 2020 Forum, p 0413
Cui T, Zheng Z, Wang P (2020c) Surrogate model assisted lithium-ion battery co-design for fast charging and cycle life performances. In: ASME 2020 international design engineering technical conferences and computers and information in engineering conference. American Society of Mechanical Engineers Digital Collection
Deshmukh AP, Allison JT (2016) Multidisciplinary dynamic optimization of horizontal axis wind turbine design. Struct Multidisc Optim 53(1):15–27. https://doi.org/10.1007/s00158-015-1308-y
Deshmukh AP, Herber DR, Allison JT (2015) Bridging the gap between open-loop and closed-loop control in co-design: a framework for complete optimal plant and control architecture design. In: 2015 American control conference, pp 4916–4922. Chicago, IL, USA
Du X, Chen W (2004) Sequential optimization and reliability assessment method for efficient probabilistic design. ASME J Mech Des 126(2):225–233
Du X, Guo J, Beeram H (2008) Sequential optimization and reliability assessment for multidisciplinary systems design. Struct Multidisc Optim 35(2):117–130. https://doi.org/10.1007/s00158-007-0121-7
Fan X, Wang P, Hao F (2019) Reliability-based design optimization of crane bridges using kriging-based surrogate models. Struct Multidisc Optim 59(3):993–1005. https://doi.org/10.1007/s00158-018-2183-0
Fathy HK, Papalambros PY, Ulsoy AG, Hrovat D (2003) Nested plant/controller optimization with application to combined passive/active automotive suspensions. In: American control conference. IEEE, Denver, pp 3375–3380
Fathy HK, Reyer JA, Paplambros PY, Ulsoy AG (2001) On the coupling between the plant and controller optimization problems. In: Proceedings of the 2001 American control conference, vol 3, pp 1864–1869. Arlington, VA
Forcier LC, Joncas S (2012) Development of a structural optimization strategy for the design of next generation large thermoplastic wind turbine blades. Struct Multidisc Optim 45(6):889–906. https://doi.org/10.1007/s00158-011-0722-z
Grujicic M, Arakere G, Pandurangan B, Sellappan V, Vallejo A, Ozen M (2010) Multidisciplinary design optimization for glass-fiber epoxy-matrix composite 5 mw horizontal-axis wind-turbine blades. J Mater Eng Perform 19(8):1116–1127
He Y, Monahan AH, Jones CG, Dai A, Biner S, Caya D, Winger K (2010) Probability distributions of land surface wind speeds over North America. J Geophys Res Atmos 115(D4):1000. https://doi.org/10.1029/2008JD010708
Herber DR, Allison JT (2019) Nested and simultaneous solution strategies for general combined plant and control design problems. ASME J Mech Des 141(1):011402
Hu Z, Du X (2015) First order reliability method for time-variant problems using series expansions. Struct Multidisc Optim 51(1):1–21. https://doi.org/10.1007/s00158-014-1132-9
Hu Z, Li H, Du X, Chandrashekhara K (2013) Simulation-based time-dependent reliability analysis for composite hydrokinetic turbine blades. Struct Multidisc Optim 47(5):765–781. https://doi.org/10.1007/s00158-012-0839-8
Hu W, Choi KK, Cho H (2016) Reliability-based design optimization of wind turbine blades for fatigue life under dynamic wind load uncertainty. Struct Multidisc Optim 54(4):953–970. https://doi.org/10.1007/s00158-016-1462-x
Jager D, Andreas A (1996) NREL National Wind Technology Center (NWTC): M2 Tower; Boulder, Colorado (Data). NREL Report DA-5500-56489. National Renewable Energy Lab. (NREL), Golden
Jiang X, Lu Z, Hu Y, Lei J (2021) Time-dependent performance measure approach for time-dependent failure possibility-based design optimization. Struct Multidisc Optim. https://doi.org/10.1007/s00158-020-02795-x
Jonkman J, Butterfield S, Musial W, Scott G (2009)Definition of a 5-mw reference wind turbine for offshore system development. Tech. Rep. National Renewable Energy Lab. (NREL), Golden
Karush W (1939) Minima of functions of several variables with inequalities as side constraints. MSc Dissertation, Department of Mathematics, University of Chicago
Kooijman H, Lindenburg C, Winkelaar D, Van der Hooft E (2003) Aero-elastic modelling of the DOWEC 6 MW pre-design in PHATAS. DOWEC Dutch Offshore Wind Energy Converter 1997–2003 Public Reports
Kulunk E (2011) Aerodynamics of wind turbines. In: Fundamental and advanced topics in wind power. IntechOpen, London
Lantz EJ, Roberts JO, Nunemaker J, DeMeo E, Dykes KL, Scott GN (2019) Increasing wind turbine tower heights: Opportunities and challenges. Tech. Rep. National Renewable Energy Lab. (NREL), Golden
Lee G, Son H, Youn BD (2019) Sequential optimization and uncertainty propagation method for efficient optimization-based model calibration. Struct Multidisc Optim 60(4):1355–1372. https://doi.org/10.1007/s00158-019-02351-2
Lee U, Kang N, Lee I (2020) Shared autonomous electric vehicle design and operations under uncertainties: a reliability-based design optimization approach. Struct Multidisc Optim 61(4):1529–1545. https://doi.org/10.1007/s00158-019-02434-0
Li H, Cho H, Sugiyama H, Choi KK, Gaul NJ (2017) Reliability-based design optimization of wind turbine drivetrain with integrated multibody gear dynamics simulation considering wind load uncertainty. Struct Multidisc Optim 56(1):183–201. https://doi.org/10.1007/s00158-017-1693-5
Liang J, Mourelatos Z, Nikolaidis E (2007) A single-loop approach for system reliability-based design optimization. ASME J Mech Des 129(12):1215–1224
Liberzon D (2011) Calculus of variations and optimal control theory: a concise introduction. Princeton University Press, Princeton
Lindenburg C (2002) Aeroelastic modelling of the LMH64-5 blade. Technical Report No. DOWEC-02-KL-083/0. Energy Research Center of the Netherlands
Maki K, Sbragio R, Vlahopoulos N (2012) System design of a wind turbine using a multi-level optimization approach. Renew Energy 43:101–110
McWilliam MK, Barlas TK, Madsen HA, Zahle F (2018) Aero-elastic wind turbine design with active flaps for AEP maximization. Wind Energy Sci 3(1):231

Nguyen T, Song J, Paulino G (2010) Single-loop system reliability-based design optimization using matrix-based system reliability method: theory and applications. ASME J Mech Des 132(1):011005

Noh Y, Choi K, Du L (2009) Reliability-based design optimization of problems with correlated input variables using a Gaussian copula. Struct Multidisc Optim 38(1):1–16

NWTC (2020) NWTC Information Portal (NWTC 135-m Tower Data)

Park HU, Lee JW, Chung J, Behdinan K (2015) Uncertainty-based MDO for aircraft conceptual design. Aircraft Eng Aerosp Technol 87(4):345–356

Patterson MA, Rao AV (2016) A general-purpose MATLAB software for solving multiple-phase optimal control problems, version 2.3

Pavese C, Tibaldi C, Zahle F, Kim T (2017) Aeroelastic multidisciplinary design optimization of a swept wind turbine blade. Wind Energy 20(12):1941–1953

Sieros G, Chaviaropoulos P, Sørensen JD, Bulder BH, Jamieson P (2012) Upscaling wind turbines: theoretical and practical aspects and their impact on the cost of energy. Wind Energy 15(1):3–17

Sim SK, Maass P, Lind PG (2019) Wind speed modeling by nested arima processes. Energies 12(1):69

Tu J, Choi K, Park Y (1999) A new study on reliability- based design optimization. ASME J Mech Des 121(4):557–564

Vasjaliya NG, Gangadharan SN (2013) Aero-structural design optimization of composite wind turbine blade. In: Proceedings of the 10th world congress on structural and multidisciplinary optimization, vol 21, p 2014

Wu JS, Chiang LK (2004) Free vibrations of solid and hollow wedge beams with rectangular or circular cross-sections and carrying any number of point masses. Int J Numer Methods Eng 60(3):695–718

Yan H, Yan G (2009) Integrated control and mechanism design for the variable input-speed servo four-bar linkages. Mechatronics 19(2):274–285

Youn B, Choi K, Park Y (2003) Hybrid analysis method for reliability-based design optimization. ASME J Mech Des 125(2):221–232

Youn BD, Choi KK, Du L (2005) Enriched performance measure approach for reliability-based design optimization. AIAA J 43(4):874–884

Zhang J, Gao L, Xiao M, Lee S, Eshghi AT (2020) An active learning kriging-assisted method for reliability-based design optimization under distributional probability-box model. Struct Multidisc Optim 62(5):2341–2356. https://doi.org/10.1007/s00158-020-02604-5